

Ventilation airflow around a continuous miner and its effect on methane concentrations at the face

Heather N. Dougherty P.E., MBA

Thesis submitted
to the Benjamin M Statler College of Engineering and Mineral Resources
at West Virginia University

in partial fulfillment of the requirements for the degree of

Masters of Science in
Mining Engineering

Yi Luo, Ph.D., Chair
Felicia Peng Ph.D
Brijes Mishra Ph.D.

Department of Mining Engineering

Morgantown, West Virginia

2014

Keywords: Mining, Ventilation, Methane, Continuous Miner (CM), Anemometer

Copyright © 2014 Heather Dougherty

UMI Number: 1573320

All rights reserved

INFORMATION TO ALL USERS

The quality of this reproduction is dependent upon the quality of the copy submitted.

In the unlikely event that the author did not send a complete manuscript and there are missing pages, these will be noted. Also, if material had to be removed, a note will indicate the deletion.



UMI 1573320

Published by ProQuest LLC (2015). Copyright in the Dissertation held by the Author.

Microform Edition © ProQuest LLC.

All rights reserved. This work is protected against unauthorized copying under Title 17, United States Code



ProQuest LLC.
789 East Eisenhower Parkway
P.O. Box 1346
Ann Arbor, MI 48106 - 1346

ABSTRACT

Ventilation airflow around a continuous miner and its effect on methane concentrations at the face

Heather N Dougherty

Attaining an accurate understanding of airflow distribution at the continuous miner face is instrumental in maintaining a safe mining environment. Currently, continuous miner face air readings can be taken in the last open crosscut and at the curtain mouth. By measuring airflow in a pre-determined area it is accepted that an adequate quantity of that air sweeps the face of harmful dust and gasses. Unfortunately, due to the location inaccessibility, precise face velocity readings can only be determined in a laboratory setting or through computer-simulated programs verified by laboratory models. The National Institute for Occupational Safety and Health (NIOSH) Office of Mine Safety and Health Research (OMSHR) ventilation gallery was used to simulate common ventilation scenarios and measure air velocities utilizing ultrasonic anemometers. The ventilation gallery simulates a full-scale mining face similar to a continuous miner (CM) room and pillar operation and provides a means to obtain representative air velocities in areas typically inaccessible on an actual CM face. Methane gas was also released from pipes located at the face to simulate realistic face gas emissions and dilutions.

Improving upon previous empty gallery testing and to more effectively determine representative face methane readings, a mockup of a continuous miner with water sprays and a scrubber fan was used to further refine face airflow conditions that would be closer to actual mining conditions. Throughout testing, methane was monitored along the face and at the machine-mounted monitor location allowing direct comparisons of concentrations at these critical locations. Multiple laboratory tests were run, varying parameters such as airflow quantity, entry width (sump or slab cut), and face ventilation configuration (blowing or exhausting curtain). Test data showed a similar pattern of methane concentrations at both low and high airflow quantities, but a difference in the distribution of methane concentrations between narrow and wide entry widths. As verified in previous research, most tests showed that blowing face ventilation was more efficient in diluting methane than exhausting ventilation. The patterns of airflow and methane concentrations observed in this testing can further improve the understanding of airflow in and around the CM and face, promoting effective use of face ventilation to improve the health and safety of miner.

Table of Contents

ABSTRACT	i
Figures	iii
Chapter 1: Introduction	1
Chapter 2: Literature Review.....	4
Chapter 3: Methodology	8
Variables	8
Ventilation Gallery – testing facility	10
Testing	13
Equipment	13
Test Setup	16
Laboratory Testing	19
Chapter 4: Results and Analysis	21
Data Analysis	21
Results	22
Detailed Analysis of Sump Cut, High flow scenarios.....	29
Discussion.....	34
Chapter 5: Conclusions and Recommendations	37
References:.....	39
Appendix A.....	1

Figures:

Figure 1: Ventilation Test Gallery. (Taylor, Chilton et al. 2010) Arrows indicate air direction into the gallery in a blowing curtain configuration and out through an exhaust fan. The CM is shown close to the mining face and is approximately 0.3 m (1 ft) from the face area during testing.....	10
Figure 2: Model CM machine, top and side view.(Taylor, Chilton et al. 2010).....	11
Figure 3 Water sprays on model mining machine. (Taylor, Chilton et al. 2010)	12
Figure 4. Gas manifold at the test gallery face (Taylor, Chilton et al. 2010)	13
Figure 5: The Gill 3-Axis Sonic Anemometer on a laboratory stand.....	14
Figure 6. Methane sampling system(Taylor, Chilton et al. 2010)	16
Figure 7 Support system for moving anemometer over top of miner.(Taylor, Timko et al. 2004).....	18
Figure 8: Instrument placement within the test gallery. The small numbers represent methanometer locations and the large numbers represent anemometer locations. Narrow indicates Sump Cut, while Wide indicates slab cut. Scale is in feet.....	19
Figure 9: Ultrasonic anemometer sensor heads with flow components (Taylor, Chilton et al. 2010)	21
Figure 10. Reference angle directions in degrees.(Taylor, Timko et al. 2004)	22
Figure 11: Graphical data of methane percentages for the sump and slab entry widths and showing blowing and exhausting ventilation for face methane monitoring Locations 1, 2, 3, and 4 from Figure 8. Sensor indicates the methane reading at the location of the machine-mounted methane monitor in the blowing or exhausting setup.....	24
Figure 12: Velocity direction recorded in Degrees for Location 1 of the High flow, Sump Cut, Blowing Ventilation test case. Each series represents a test and the repeats	32
Figure 13: A figure showing air velocity direction, the arrow indicates magnitude. NTS	34

Chapter 1: Introduction

The technological advancements in continuous miner (CM) machines, particularly those with remote control equipment, make mining depths of greater than 6.1 m (20 feet) - deep-cut mining, standard in underground coal mining. Deep cuts improve production rates but can also hinder fresh air from getting to the cutting face. It is important to understand the ventilation in and around the mining face so that preventative measures are taken to ensure air flow to the face for diluting the methane emitted during mining.

Methane, a naturally occurring coalbed gas is adsorbed into the solid coal matrix and exists in fractures in the coal or other surrounding rock is released during mining. When released from the coal during mining, if not properly diluted by ventilation air, methane in some zones can reach its explosive concentration to create a potentially hazardous environment.

However, the insufficient dilution problems could occur when coal mining operations are conducted with increased cutting depth, increased speed of mining cycles, and deeper mining depths. The foremost problem includes increased methane liberation within deeper coal beds and ventilation capacities being stretched to their limits. These complications can hinder getting adequate ventilation to the face for the dilution of methane gas.

All underground bituminous coal mines are considered gassy by the Mine Safety and Health Administration (MSHA) (CFR 2011) and have specific stipulations for minimal ventilation air required at the CM mining face. Historically, the designs and regulations for ventilating CM faces were developed for the standard maximum of a 6.1 m (20 foot) cut. MSHA has determined that 0.3 m/s (60ft/min) of ventilation air is a basic minimum at the face where coal is being cut (CFR 2011) §75.326. As mines grow larger and increase cut area in the entry this can lead to a need for a greater volume of air to attain the required 0.3 m/s (60 ft/min) at the measurement point. With increased mining depths and mining speed, methane liberation is amplified and it consequently leads to the need to improve the ventilation air flow and efficiency.

Ventilating the face to sweep away dangerous contaminants, such as methane, is crucial to the health and safety of mine workers. Title 30 Code of Federal Regulations (CFR 2011) part 75.342 stipulates that when the methane concentration reaches 1.0 percent, the monitor shall give a warning signal to a person who can de-energize the affected electric equipment or shut down the diesel-powered equipment. When the concentration at any methane monitor reaches 2.0 percent, the monitor “shall automatically de-energize the electric equipment or shut down the diesel-powered equipment on which it is mounted.”(CFR §75.342(c)1) These regulations require methane monitors to be installed on all face machinery that cut or load coal, and to be placed “as close to the working face as practicable” (CFR §75.342(a)3). Because the machine-mounted methane monitor is not located on the face where methane concentration can be highest, its readings may not always reflect actual gas readings at the face. Since as early as the start of CM there have been concerns about the methane produced at the face exceeding the lower explosive limit (LEL) even when the average concentration was within standard limits (Kissell, Banfield Jr et al. 1974). Therefore, it is important to understand how airflow is coursed and how best to ventilate the deep cut face area for sweeping the contaminants away so that a safe operating condition is maintained.

A major problem associated with deep cut mining is the risk of methane explosions. An explosion in underground coal mine depends on three key elements in an underground coal environment, between 5-15% methane concentration, oxygen, and an ignition source. Reducing or removing one of these basic elements is the key to reducing the likelihood of the explosion risk. Oxygen is a mandatory condition of human operation within the mining atmosphere, and therefore cannot be taken out of the matrix. Ignition sources such as the electrical power and the sparks created by metal cutting head striking hard material are also difficult to mitigate. Regular cutter bit changes and not allowing them to get dull has been found to reduce sparks (Colinet, Listak et al. 2010). Electrical power is standard in most mining equipment applications for cutting equipment, auxiliary ventilation, coal haulage devices, and belt conveyors. Although electrical standards are mandated to keep this equipment intrinsically safe in high risk areas. Methane, a byproduct of the mining process, can be diluted to non-explosive ranges using proper ventilation. Methane is the easiest source that can be monitored and manipulated to

reduce the risk of explosions at the CM mining face and is controlled by the ventilation air. Ventilation is the most controllable component to create a safer environment for miners on the CM face. Ventilation has been studied in several ways to increase the safety of the face area for the deep cut. Understanding and controlling air at the CM face can assist in creating a safer and more productive mine.

The objective of this work is to further the understanding of airflow in the CM working face. The research is a continued effort beyond the airflow study in an unoccupied entry work done previously by NIOSH. The experimental studies were conducted in a ventilation test gallery with a full-scale CM model placed in various possible locations. Blowing and exhausting curtain ventilations were provided to the gallery. The data generated from an intensive ventilation monitoring program enable the examination of both airflow and methane distributions at the face and around the CM. Airflow in the ventilation gallery was analyzed in different set up scenarios. The effectiveness of ventilation was determined by methane concentrations and airflow velocity. This information can be used to improve awareness of hazardous conditions at the CM mining faces, thus reducing the risk of methane ignition.

Chapter 2: Literature Review

In early literature about ventilation in continuous miner places, it was initially determined that the percentage loss of air between the curtain and the face was often greater than that of the whole ventilation system (Stahl 1958, Schlick and Dalzell 1963). It was necessary to extend the line brattice as close to the mining face as possible to direct the air to the mining face to improve airflow to the face. Auxiliary ventilation using tubing and exhaust fans were later used to promote the air sweeping across the face. Schlick (1963) discussed using push and pull ventilation by the use of tubing and a machine-mounted diffuser as auxiliary ventilation to assist in the air sweeping the face and diluting methane. CM sprays and scrubbers were not discussed, and the machine mounted diffuser appears to be the initialization of a scrubber system for the CM. Although at the time, it was stated that dust was a major issue with mining and ventilating the CM face (Stahl 1958, Schlick and Dalzell 1963).

There has been much research into ventilation on the CM face for dust, air flow and methane mitigation. Much of the work done in dust control concentrates on the innovations of machine mounted scrubbers, water sprays, and ventilation for reduction of respirable dust and concludes that the addition of these systems improves fresh air flow at the face (Volkwein and Thimons 1986, Taylor and Goodman 1997, Thimons, Taylor et al. 1999). It was found that the machine mounted scrubbers, used to reduce respirable dust by collecting dust from the air before it can reach the miner operator also assists in ventilating the face with increased brattice setbacks and assisted in diluting methane (Volkwein and Thimons 1986). Sprays are used to wet the coal for transportation to reduce dust and also assist in the airborne capture of dust at the cutting face (Kissell 2003). Dust control by spray has looked into the placement of these sprays on the CM, and although there are some areas that are more effective at reducing dust, maintenance implications can determine where sprays will be more likely to function on a regular basis (Matta 1976). For example, sprays under the boom have been determined to be more effective, but because damage is more likely in this region, it is more commonly seen that the sprays are placed on the top of the boom. Type of water spray nozzle, water pressure, spray location and number of sprays are all

characteristics of applications of sprays to reduce dust (Colinet, Listak et al. 2010). Various cone spray nozzles, pressures and water flow was compared to determine the air moving effectiveness of the parameters (Colinet, Listak et al. 2010). Taylor showed that the operation of water sprays does not significantly increase the volume of air reaching the face, but does direct the air across the face and improves mixing of the methane and the intake air at the face (Taylor, Chilton et al. 2010).

Additionally dust control parameters on CM faces include the operation of a machine mounted scrubber. Machine mounted scrubbers carry air from the face through ductwork within the miner and filter the air before it is released out of the back of the miner into the entry. Scrubbers, which when used effectively by approximately matching the scrubber flow with the intake flow can be an effective way to get intake air to the face and reduce methane concentrations. Although Taylor showed that regardless of the intake air flow, if the scrubber flow is increased the face methane will be reduced if recirculation is controlled by minimizing leakage around the curtain, and directing the scrubber exhaust away from the blowing curtain (Taylor, Chilton et al. 2010).

Taylor (2010) researched the effects of scrubber flow and water sprays on face ventilation flow, finding that scrubber use increased the amount of intake airflow reaching the mining face. They also examined the effect of curtain setback distance and its effect on face airflow and methane concentration. Proving that the closer the curtain is to the face, the better the dilution of methane, and quantity of air at the face. Previous ventilation gallery research has measured flow direction at various points within the empty entry to record ventilation velocity and direction (Taylor, Chilton et al. 2010). Methane concentrations were also logged and mapped, showing the influence of the ventilation on the methane concentrations in the empty entry.

Getting airflow to the face is of utmost importance to mine gassy coal quickly and successfully. Measuring of airflow accurately is important to achieving this aim for monitoring and altering of the airflow to the face to mitigate gas issues. Airflow has been measured in United States coal mines by the standard mechanical rotating vein anemometer using a zigzag transverse and is used as the standard airflow

measurement equipment. Their use has been standard for over a century because of their ease of use, they give an on the spot reading of air flow, their small easy to transport size, and they can be used throughout the mine without the need for electricity. Some issues with the rotating vein anemometer is that the effects of dust can affect the performance as well as pulsing airflows and human error. Measurement of differential pressures is taken with a standard Pitot tube or manometer to calculate flow in tubes, regulators or fans. There have been many ways that engineers measure airflow in mines, some of the various ways include visible tracers including historically candles and smoke, chemical smoke tubes, gases tracers, streamers, Velometer, mechanical rotating vein anemometer, electrical sensing vein anemometers, vortex shedding flow sensors, pressure differential anemometers, hot wire anemometers, and ultrasonic are some devices that have been used (Unwin November 2007).

Other experimental ways to measure airflow on CM faces have been presented in research. Since measuring air flow and methane at the face is not possible in real mining situations because of roof control and safety issues, other methods have been developed to simulate this environment to better determine ventilation in this area. Full scale models of a CM face as in this research have been utilized experimentally to determine flow around the miner at the CM face, in the cut, methane and dust concentrations under controllable variables (Volkwein and Thimons 1986, Goodman and Taylor 1993, Thimons, Taylor et al. 1999, Taylor, Timko et al. 2004, Wala, Vytla et al. 2007, Taylor, Chilton et al. 2010). These full scale tests have also been integrated with other methods to cross verify methods primarily computational fluid dynamic and computer modeling. Other methods that have been used are scaled physical models and particle image velocimetry in laboratory setting also combined with full scale and computer modeling (Wala, Vytla et al. 2007).

Computational fluid dynamics (CFD) was utilized to model an empty entry (Wala, Vytla et al. 2007), validating NIOSH laboratory data. This was considered the first full scale CFD validation study. Air flow and methane concentration readings were not taken simultaneously due to safety concerns. It was proven, for these examples that with the validation information from the full scale test, CFD models were in good agreement

(Wala, Vytla et al. 2007). Wala progressed to gathering methane data from the NIOSH test facility with the mock miner in place at the face and the scrubber on in various levels, comparing methane concentrations to CFD models(Wala, S et al. 2008). Hargreaves and Lowndes (2007) also utilized CFD to model face ventilation using tubing in a blowing face configuration. They showed ventilation patterns of airflow in various stages of cutting and bolting, finding CFD to be successful in identifying the ventilation characteristics associated with various auxiliary ventilation systems during a typical mining cycle. More recently Petrov, using CFD modeling, and small and large scale modeling developed a passive regulator that can assist in intake air penetration to the face (Petrov and Wala 2014). CFD is a powerful computer based tool that can predict detailed flow patterns to assist in the planning and variation of detailed ventilation at CM faces. Validation of these CFD models with full scale testing is imperative to good authentication of the CFD program.

Chapter 3: Methodology

Variables

Two common practices of ventilating a CM face are blowing and exhausting ventilation. When implementing blowing ventilation the intake air is delivered to the face of the working CM entry by blowing it from behind a line brattice curtain or tubing. This intake air is blown at a higher velocity than the exhaust curtain due to the smaller area towards the face and sweeps away the face contaminants and is then exhausted in the entry towards the return. This system encourages the miner operator to be positioned behind the blowing curtain in the clean air while mining is taking place. Although this method is the most commonly used and most effective way of ventilating the face (Taylor, Chilton et al. 2010) it positions other mobile equipment operators like the shuttle car and roof bolters downwind of the CM in the return air. It also can restrict the movement, and possibly the visibility of the face to the continuous miner operator, due to the need to be in the fresh air while mining.

When implementing exhausting ventilation on the CM face, the intake air is delivered to the face from the working entry. The intake air sweeps the face, and the contaminant laden return air then is drawn behind the return curtain or through exhaust tubing to the return entries. This system allows all of the mobile equipment to be in the fresh air and allows the continuous miner operator to have more freedom of movement within the entry than with the blowing system. Both of the blowing and exhausting systems have various advantages and disadvantages and can be successfully implemented when a mining plan is determined and implemented.

Both water sprays on the CM machine and head and a scrubber fan system were used in this testing. These systems are a part of all CM mining best practices due to the fact that they minimize respirable dust and assist in diluting methane and directing ventilation air at the face area. CM machine sprays were consistent throughout experiments, with the flow and psi not varied with any testing, and just considered “on”. Machine water sprays additionally act as a cooling and wetting agent which can reduce the potential for frictional ignitions. The machine scrubber flow was varied by orface

plates on the front of the machine to reduce or increase flow to approximately match the flow of the intake air measured behind the curtain. Matching of these two values is considered a best practice due to the fact that it discourages recirculation of the return air to the face.

A common miner was used in this testing, which cuts a 5.0m (16.5 ft) entry width in two cuts. This miner cuts initially a sump cut into the solid coal face, approximately 4.0m (13.0 ft) wide to a depth of approximately 12.2m (40 feet). It then backs out of this position, re-positions to the “slab” of coal that is 1.0 m (3.5 feet) wide and cuts this Slab cut to make then entry approximately 5.0m (16.5 feet) wide. Wider entries can be cut, full face miners are used, and wider entries are sometimes used in various mining configurations. The situation of a sump and slab cut with a maximum entry width of 5.0m (16.5 feet) was chosen due to the limitations of the NIOSH ventilation gallery.

Placement of the sonic airflow sensor placement in this study was limited by the current set up in the laboratory and equipment itself. These initial measurements, once studied with computer modeling will detail future locations for sensor placement in studies. Placement over top of the miner was identified as a prime location for information gathering of flow parameters in that area. Points behind the blowing or exhausting curtain were of importance as to monitor total flow that is getting to the CM face area. Locations behind the miner were meant to relay information on the airflow behind the miner in the entry.

Methane sensor placement was determined to be 0.3 m (1 foot) from the roof and 0.3 m (1 foot) from the face. This was decided because the methane is released from the face, and it is lighter than air, so a higher placement of sensors should gather information on the highest methane concentrations across the face. The division of the sensors along the face were due to other research placement of sensors, so that a comparison could be done (Taylor, Chilton et al. 2010) in the future if needed for calibration of computer modeling. The last methane sensor was placed in an area that would be similar to a machine mounted sensor placement on the mining equipment. This allowed comparison to what a miner would be reading on the equipment and what was actually being released from the mining face.

Ventilation Gallery – testing facility

The ventilation test gallery is located at the NIOSH facility in Bruceston, PA, is an L-shaped building designed to mimic a CM face (**Figure 1**). The test gallery is a maximum of 2.1 m (7 ft) high and 5.0 m (16 ½ ft) wide. Entry width can be varied from 4 m to 5 m (ft) by moving walls made of curtain and wood. The ceiling and walls are covered in rough concrete material to simulate real world mine surfaces. The face of the test gallery is an airtight wall built across the entry with a gas manifold installed for uniform methane distribution (Figure 4).

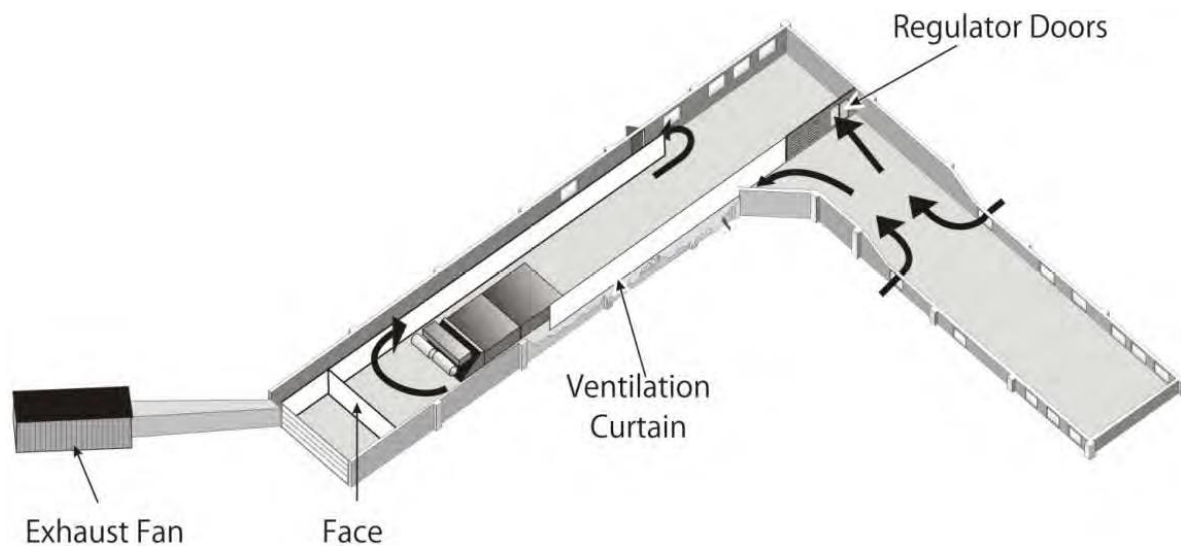


Figure 1: Ventilation Test Gallery. (Taylor, Chilton et al. 2010) Arrows indicate air direction into the gallery in a blowing curtain configuration and out through an exhaust fan. The CM is shown close to the mining face and is approximately 0.3 m (1 ft) from the face area during testing.

A vane-axial exhaust fan located outside the test gallery has a flow capacity of 5.9 m³/s (12,500 ft³/min) and draws intake air through openings in the back of the test gallery. Tests can be conducted with either blowing or exhausting face ventilation by changing the curtain configuration within the laboratory. Airflow is varied by opening or closing regulator doors as shown in **Figure 1**. Curtain setback distance can be varied using wood frame and brattice removable walls. For this testing a curtain setback distance of

Systems, Co. hollow cone water spray nozzles were mounted on top of the miner using 3-m (10-ft) long plastic pipe operating at 0.48 MPa (70 psi) water pressure and angled at approximately 30 degrees in the direction of the airflow sweeping the face from left to right.. In addition, four hollow cone nozzle sprays on each side of the CM spraying into the face were used spraying directly on the face to mimic mining situations. A schematic of the water spray set up is seen in **Figure 3**

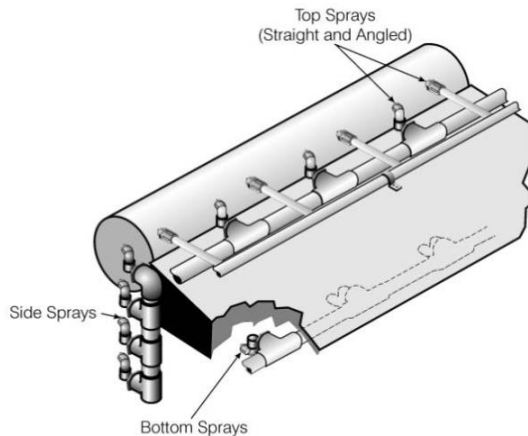


Figure 3 Water sprays on model mining machine. (Taylor, Chilton et al. 2010)

Figure 4 represents a uniform methane release from the test gallery face was simulated by a manifold system consisting of four horizontally positioned 3.8-cm (1.5-inch) diameter copper pipes located 0.1 m (4 inches) away from the face. The four pipes were equally spaced in the 2.1-m (7-ft) high face area and were perforated on the top and bottom with 2-mm (1/16-in) diameter holes placed 50 mm (2 in) apart. Original length of the pipes for the 4.0 m (13 ft) face is 3.0 m (10 feet). Extension pipes were added when the face width changed from 4.0 m to 5.0 m (13 ft to 16.5 ft) during the slab cut extending the pipes to approximately 3.6 m (12 feet). Gas flow rates were set using a flow meter and could be varied from 3.8 to $16.5 \times 10^{-3} \text{ m}^3/\text{s}$ (8 to 35 cfm). A methane flow of $8.5 \times 10^{-3} \text{ m}^3/\text{s}$ (18 cfm) was maintained during testing to keep the methane levels in the ventilation gallery below two percent due to safety concerns. A commercial natural gas source of approximately 99 percent methane was used for testing.

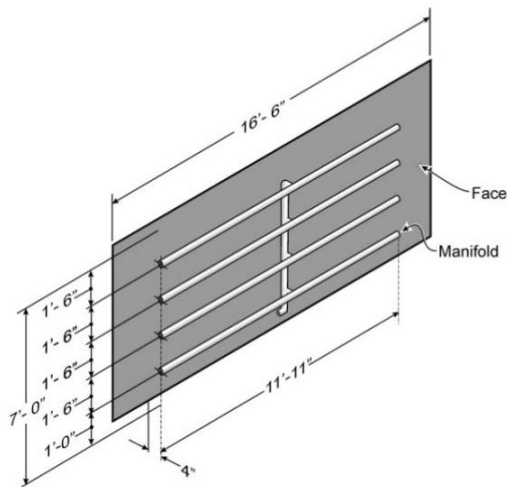


Figure 4. Gas manifold at the test gallery face (Taylor, Chilton et al. 2010)

Redundant safety precautions are taken within the ventilation gallery due to the use of methane in testing. All work is planned with the maximum methane in any monitored location to be 2.0% or less. Gallery safeguards include an automatic gas shut off if the main gallery fan is not in operation, strobe lights on the gallery to alert others in the area that methane is being used within the laboratory, and an automatic shut off if there is power on within the gallery. All power must be off when methane is being used in the gallery. Due to this safeguard, ventilation air flow and methane were monitored separately.

Testing

Equipment

Ultrasonic anemometers as shown in **Figure 5** are designed for measuring velocity in a two- or three-dimensional space. These anemometers are robust, are easily adaptable to changing environments, and are used extensively in meteorological applications. Gill ultrasonic anemometers were used for acquiring air velocities in the ventilation test gallery. These anemometers have been successful in laboratory testing due to their ease of use and lack of required calibration when moved to different locations (Martikainen, Dougherty et al. 2010, Martikainen, Taylor et al. 2011). The measurement of air velocity vectors is based on the speed of the sound pressure wave and distance

between the sensor heads. The ultrasonic anemometers chosen were Gill Windmaster (2011) instruments, which measure air velocity and direction in all three axes. The instrument has a velocity range of 0-45 m/s (0-8,900 fpm) with a resolution of 0.01 m/s (2.0 fpm) and a direction range of 0-359° with a resolution of 0.1°. They are powered by a 12-volt power source and data is recorded from the instrument through a cable to a power communications box by a RS232 connection. This box is then connected via an Ethernet cable to an Ethernet hub, for use with multiple instruments, and finally to the laboratory computer data acquisition system.



Figure 5: The Gill 3-Axis Sonic Anemometer on a laboratory stand.

Procedures were developed for use of these ultrasonic instruments for measuring both airflow direction and velocity in the ventilation test gallery (Taylor, Chilton et al. 2002, Taylor, Chilton et al. 2002, Taylor, Timko et al. 2004, Hall, Taylor et al. 2007, Taylor,

Timko et al. 2007, Taylor, Chilton et al. 2010). Each instrument was manually placed in test locations as indicated by the large numbers in **Figure 8**. A total of four 3-axis Gill Windmaster ultrasonic anemometers were used during testing and were moved to multiple locations within the laboratory to measure additional test locations.

Methane concentrations can be monitored simultaneously at up to 16 locations in the ventilation test gallery. For these tests, only 5-6 methane sampling locations were chosen dependent on the width of the face. These testing locations were chosen to allow for close examination of maximum methane concentration areas in relation to air velocity sensor readings. Plastic tubing was connected to a vacuum pump, which draws air samples from each sampling location within the test gallery to an individual Bacharach CE130 combustible gas detection transmitter located outside of the test gallery. Each air sampling tube is the same length with an metal end piece on the tube on the laboratory end to discourage water from being gathered in the lines and progressing to the methane sensors as seen in Figure 6. Water separators are also located outside of the laboratory, connected prior to the sensors, to further verify that water does not reach the methane sensors. Methane sensors were calibrated weekly unless a discrepancy was found between multiple runs of the same test parameters.

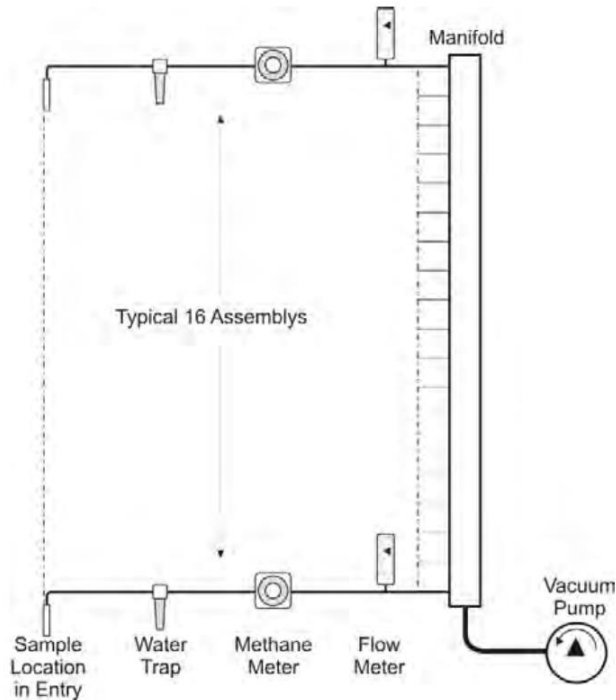


Figure 6. Methane sampling system(Taylor, Chilton et al. 2010)

A LabVIEW (2012) data acquisition program was created, called Mine Ventilation Acquisition System (MVAS), to simplify test data collection from anemometer and methanometer locations within the laboratory. Information that was inputted and saved in MVAS was location in the X,Y, and Z plane of each of the air velocity sensors and methane monitors, water pressure, intake velocity, scrubber velocity, and curtain location and configuration. Test time, airflow velocities, water pressures, and methane concentrations were collected; data was stored and transferred to a Microsoft Excel file for processing and analysis.

Test Setup

Testing criteria chosen and factors that were varied were curtain location, intake air and scrubber flow rates, and entry cut (or width). Intake flow rate at a high flow rate of approximately $4.7 \text{ m}^3/\text{s}$ (10,000 cfm) was chosen, the range that was read by the instruments was between $3.8 \text{ m}^3/\text{s}$ to $5.3 \text{ m}^3/\text{s}$ (10,500-14,700 cfm). The low flow setting of $2.0 \text{ m}^3/\text{s}$ (6,000 cfm) was chosen, and was recorded at a range of $2.3 \text{ m}^3/\text{s}$ to $3.5 \text{ m}^3/\text{s}$ (6,300-9,600 cfm) by the instruments. The airflow data shows more variation

than was actually encountered during testing because the recording instrument takes a point reading rather than a full-entry cross section reading. The anemometer that was placed behind the curtain was placed at a centerline, which is known to have the highest ventilation velocity due to less friction from the ribs being at the furthest point away from them. An additional variation in intake air quantities occurred because initial airflow settings were made before the scrubber fan on the CM was turned on. Face airflow velocity was continuously recorded behind the face curtain 0.6 m (2.0 ft) away from either the left or right rib. The face curtain was placed on the left side of the entry for blowing face ventilation or on the right side for exhausting face ventilation. A two-step extraction sequence was assumed whereby the first or sump cut was 4.0 m (13 ft) wide, followed by removal of the slab to make the final entry width of 5.0 m (16.5 ft). For all tests, curtain setback distance was 10.7 m (35 ft), water spray pressure was 70 psi, water sprays on the top of the boom were angled approximately 30° pointing to the right side of the face, and the dust scrubber was “on.” Scrubber flow was adjusted to be approximately equal to the intake airflow quantity. A test matrix of the six variables is shown in Table 1. The eight tests were run and repeated twice, for a total of three test duplications of each setup. One set of test iteration data was corrupted within the file and could not be processed, the two iterations of this test were analyzed.

Table 1: Test matrix for gallery testing

Test #	1	2	3	4	5	6	7	8
Airflow Quantity								
High (4.7 m ³ /s)	X	X	X	X				
Low (2.0 m ³ /s)					X	X	X	X
Ventilation Setup								
Exhausting face curtain	X	X			X	X		
Blowing face curtain			X	X			X	X
Entry Width								
Second/slab cut	X		X		X		X	
First/sump cut		X		X		X		X

Four ultrasonic anemometers were used for testing as seen in **Figure 9**. Ten to eleven air flow test locations were used depending upon the entry width as shown in **Figure 8**. Each setup was run multiple times due to the limited number of instruments, with the anemometers moved to different locations to complete each test. Two units were placed above the CM machine and located 0.8 m (2.5 ft) below the roof and 0.9 m (3 feet) from each edge of the CM with 1.2 m (4 feet) between each as seen in **Figure 8**. The anemometers were then moved to locations 3.7 m (12 feet), 6.1 m (20 feet), and 8.5 m (28 feet) back from the mining face. The anemometer locations above the miner were mounted upside-down to a garage door frame and moved along the installed tracks as seen in **Figure 7**. The CM location is indicated by the shaded area in **Figure 8**. The 3.7-m (12-ft) distance from the face was chosen as the closest point so that the water sprays would not directly affect the readings of the ultrasonic anemometers (Taylor et al., 2010). Another ultrasonic anemometer was placed behind the curtain 3.0 m (10 ft) from the curtain mouth to measure the total gallery flow (Location 11 in the exhausting, and Location 7 in the blowing setup in **Figure 8**). This anemometer was stationary throughout testing, placed on a stand 1.1 m (3.5 ft) from the floor, and 0.3m (1 ft) from the rib. The fourth anemometer was placed on a stand in three or four different locations behind the miner, 1.5 m (5 ft) outby the end of the curtain and 1.1 m (3.5 ft) high (Locations 7-10 or 8-11 in **Figure 8**).

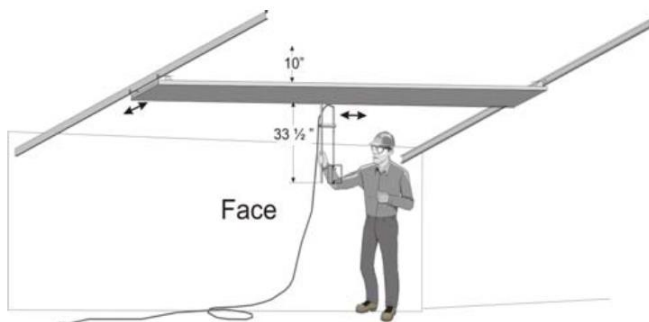


Figure 7 Support system for moving anemometer over top of miner.(Taylor, Timko et al. 2004)

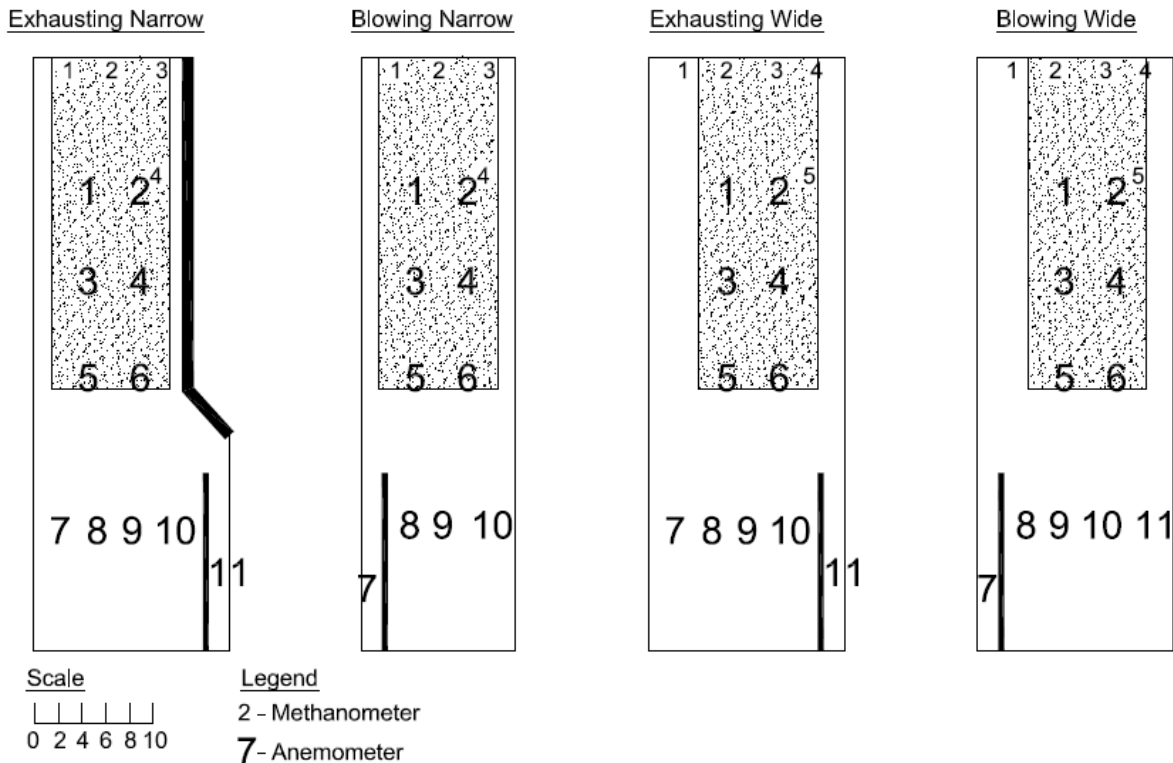


Figure 8: Instrument placement within the test gallery. The small numbers represent methanometer locations and the large numbers represent anemometer locations. Narrow indicates Sump Cut, while Wide indicates slab cut. Scale is in feet.

Methane sampling tubes were placed 0.3 m (1 ft) from the roof and 0.3 m (1 ft) from the face. For blowing or exhausting face ventilation with the sump cut entry, three sampling tubes were placed along the face and another at the standard machine-mounted methanometer location on the CM, located 2 m (7 ft) from the face and 1 m (3 ft) from the roof on the right side of the machine (Location 4 in the slab cut; Location 5 in the sump cut in Figure 8). For the slab cut scenarios, a fourth methane collection tube was added at the face.

Laboratory Testing

Test airflow measurements were recorded for approximately three minutes at a sample rate of once per second. After moving the anemometers, airflow was stabilized and the data recording was re-started. Ventilation data was recorded in vectors, with

components in the horizontal plane used to calculate flow and direction. Although the three-axis instrument also measures flow in the vertical direction, velocities were only calculated in the horizontal plane. All anemometers were situated with the North arrow pointing towards the face. Figure 10 shows the reference directions in degrees referencing the face.

A constant methane flow of approximately 18 cfm was maintained by monitoring a flowmeter and rotometer. To ensure thorough mixing, methane was released into the gallery for approximately five minutes to establish steady-state conditions before recording methane readings once per second for approximately 10 minutes. Once recording of methane data was complete, the methane was turned off, and we allowed the methane to be eliminated from the laboratory by monitoring the sensors before we re-entered and turned electrical power on.

Both ventilation and methane data from each test was compiled into one excel file. Histograms were compiled and were used to determine that the data was valid, and the mean, median, and mode were found (See Appendix A for all Statistical calculations, histograms and graphs for all locations for Blowing ventilation, High flow, Sump Cut). Maximums and minimums were also noted and analyzed.

Chapter 4: Results and Analysis

Data Analysis

Air flow data was recorded for an approximately three minute sampling period, recording one value per second (180 data points) as determined in testing protocol for ultrasonic laboratory testing (Taylor, Timko et al. 2004). This data was recorded in three directional vector components (U,V and W). These three components are orthogonal and correspond to flow in what we would refer to the X, Y, and Z directions (**Figure 9: Ultrasonic anemometer sensor heads with flow components**Figure 9). The U, or X (0 to 180) direction corresponding to flow toward and away from the face, to the right and left across the entry recorded in the V or Y (90 to 270) as in Figure 10 direction, and up and down referring to the W or Z direction (Taylor, Timko et al. 2004). UVW mode was used on the ultrasonic anemometers and data was recorded in vector form for UVW directions if available. The data was then transferred to an excel spreadsheet where the data was calculated to determine flow magnitude and direction at each point in Figure 8 in the X and Y (UV) directions. The mean of this data was taken for each test iteration and was then averaged with the reiterations of the tests. Histograms and statistical analysis of the data was created to determine if the velocity data was statistically normal, please see Appendix A for the detailed analysis of one of the tests.

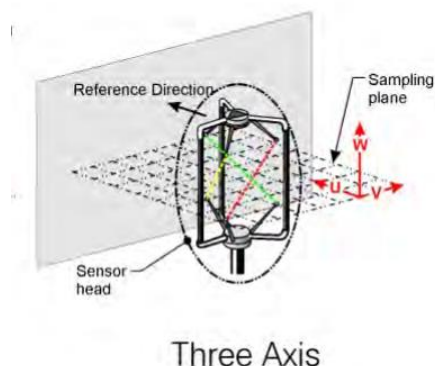


Figure 9: Ultrasonic anemometer sensor heads with flow components (Taylor, Chilton et al. 2010)

Methane data was recorded in all of the locations in the same test. Methane samples were taken once per second, but the test was run for approximately 10 minutes (approximately 600 sample readings).

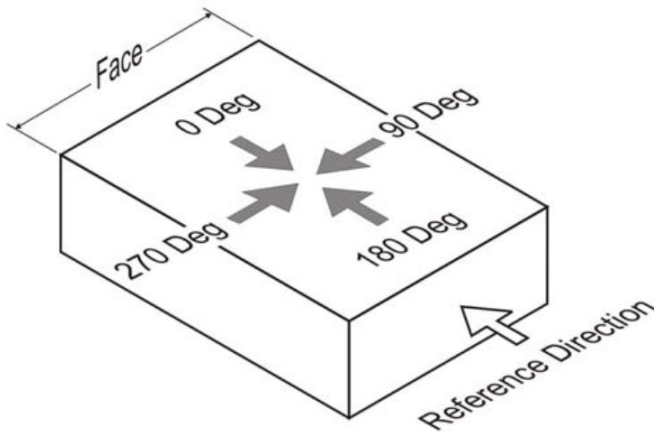
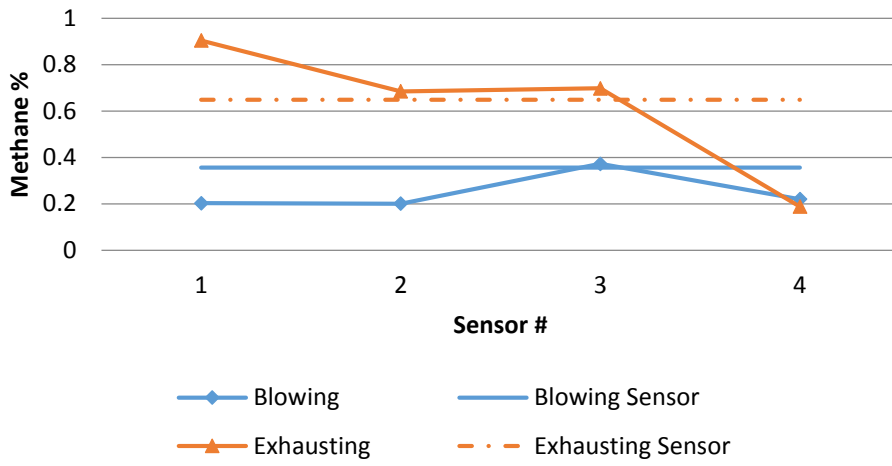


Figure 10. Reference angle directions in degrees.(Taylor, Timko et al. 2004)

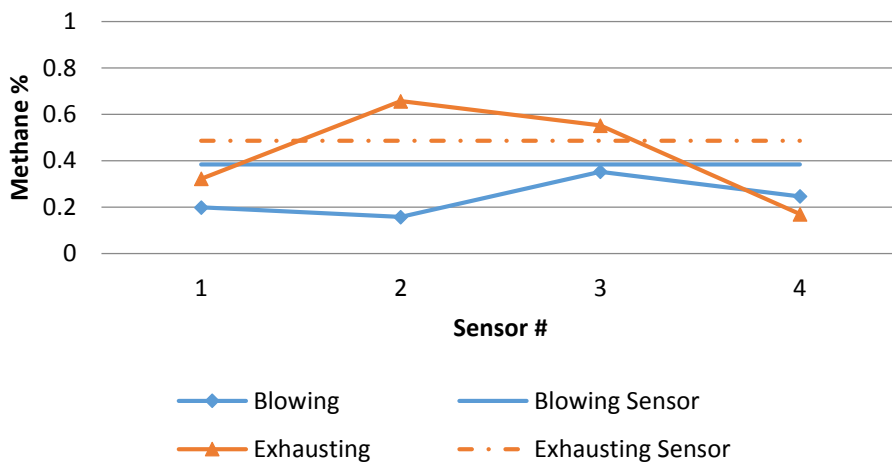
Results

Methane data was analyzed to determine which ventilation setup has the most efficient face airflow configuration. The minimum methane concentration at any location when compared to the other setups determined the best scenario, giving an indication of airflow effectiveness close to the face. Distribution of the methane along the face also allows estimation of airflows close to the face, identifying areas of lower flow by presenting higher concentrations of CH_4 . Figure 11 shows methane data as recorded for all test locations and compares blowing to exhausting ventilation. In Figure 11, the dotted line indicates the reading at the CM machine sensor location for the exhausting ventilation case, and the solid line indicates the sensor location reading for the blowing ventilation case.

11A: Slab, Low Flow



11B: Slab, High Flow



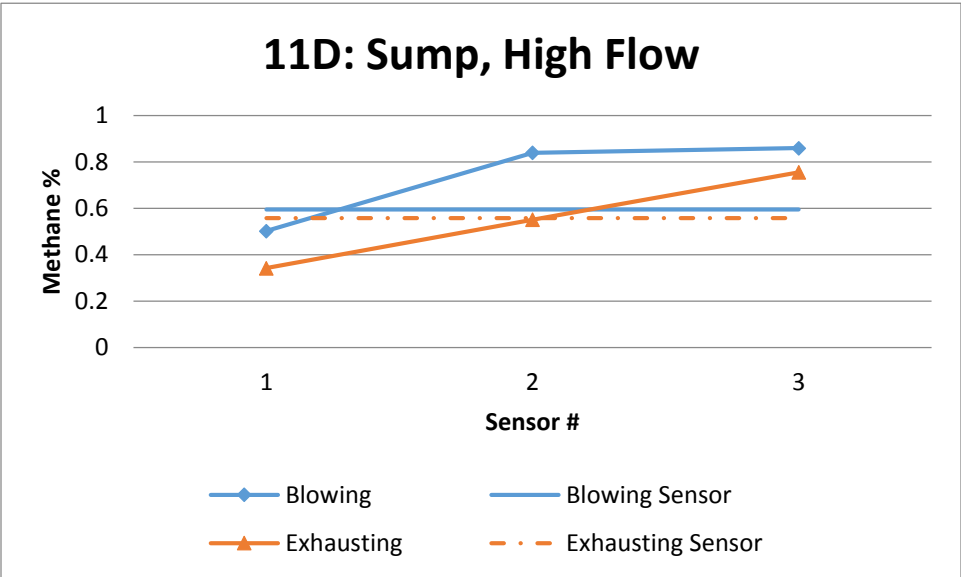
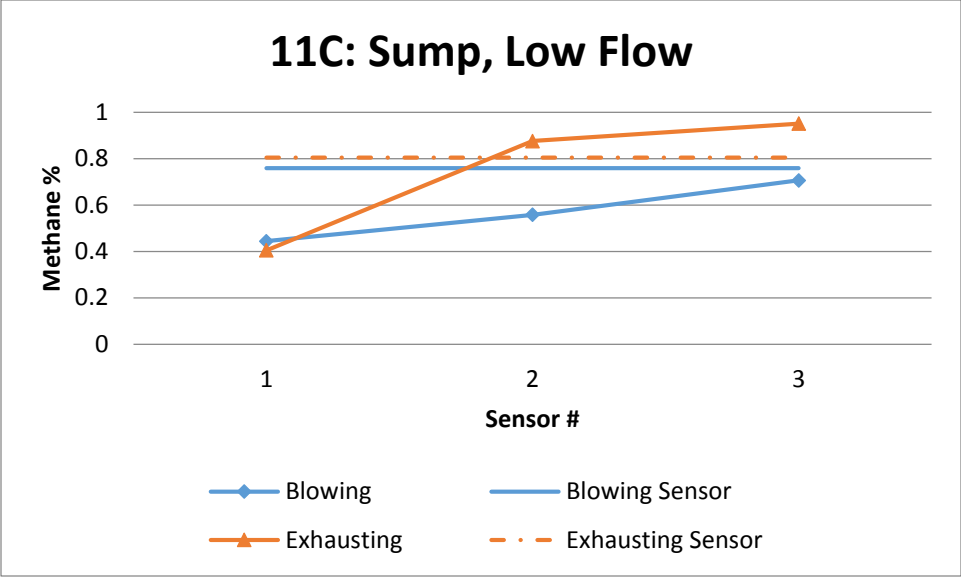


Figure 11: Graphical data of methane percentages for the sump and slab entry widths and showing blowing and exhausting ventilation for face methane monitoring Locations 1, 2, 3, and 4 from Figure 8. Sensor indicates the methane reading at the location of the machine-mounted methane monitor in the blowing or exhausting setup.

Methane concentration data for the sump cut in **Figure 11C** and **Figure 11D** show that the highest concentration was recorded in the right corner of the face (Location 3 from Figure 8) while **Figure 11A** and **Figure 11B** show that for the slab cut this corner showed a much lower face methane reading (Location 4 from Figure 8) when compared to other readings across the face. A possible cause is ventilation air flowing strongly

with a higher velocity from left to right in the sump cut, contributing to the higher methane concentration on the right side, similar to an empty entry observed by Taylor (Taylor, Chilton et al. 2010). In the wider entry or slab cut, this same pattern was not consistent. The slab cut consistently has higher methane concentrations than the sump cut, most likely due to the larger area of the cut.

Table 2 compiles velocity data for all locations from **Figure 8**, showing in all cases that the left side location closest to the face (Location 1) has a higher velocity than the right side (Location 2). Kissell (1979) demonstrated that water sprays act as small air-moving fans, directing air across the face from left to right; therefore this type of result would be expected. In most other locations above the mining machine, velocity was higher on the left-hand side during both blowing and exhausting ventilation scenarios. This could be due to the scrubber system taking a portion of the intake air from the face before it completes a sweep across the face or because the anemometer locations were outby the scrubber inlets. The blowing ventilation, sump cut case in both high and low flow were the only scenarios that showed a difference in the two locations above the CM at 6.1 m and 8.5 m (20 ft and 28 ft) outby the face, or off curtain side (**Figure 8** Locations 3-4 and 5-6). Each showed a higher velocity on the right-hand side than on the left side, but still with a higher velocity 3.7 m (12 ft) from the face on the left-hand side or curtain side (Location 1 from Figure 8).

All intake air within the system was assumed to have flowed into the scrubber system and exhausted out of the back of the CM machine. In all blowing and exhausting cases, locations behind the miner (**Figure 8** Locations 7-10 or 8-11) showed ventilation air flowing towards the face, most likely due to these locations being only 1.5 m (5.0 ft) outby the end of the curtain. Anemometer placement did not detect the scrubber exhaust, directed outby or away from the mining machine mainly due to the fact that the anemometer reading location was above the scrubber exhaust.

Air velocity direction was computed for all points and all tests, but was not analyzed with the methane and velocity data. In the detail analysis section of this Thesis information for one of the tests is discussed for all components, methane, velocity and air direction. With additional information for this test in Appendix A.

Table 2 shows that in most cases exhausting ventilation has a higher mean velocity airflow than blowing in recorded location, but does not necessarily indicate that it is more effective at ventilating the CM face. Methane readings in Figure 11 prove this otherwise. Various reasons why the flow is higher could be that the velocity of the air behind the curtain varies and at times the exhausting curtain had higher mean velocities, which can lead to higher velocities at points within the laboratory. Additionally the points chosen to record velocity readings may not be able to acquire some of the flows accurately around the miner. The current data should be used to validate a CFD model which can then lead us to establishing better locations for recording ventilation readings, permitting us a better understanding of airflow around the CM miner and face.

Table 2: Mean ventilation velocity at locations in meters per second from locations in Figure 8. Highlighted velocities are behind the curtain values.

Entry Width	Ventilation Setup	Flow	Location										
			1	2	3	4	5	6	7	8	9	10	11
Slab Cut	Blowing	Low	0.49	0.21	0.46	0.35	0.48	0.48	2.46	0.29	0.39	0.39	0.70
		High	0.87	0.30	0.78	0.73	0.94	0.76	3.81	1.79	2.36	2.05	1.48
	Exhausting	Low	0.90	0.54	0.79	0.35	0.81	0.40	1.14	0.53	0.39	0.35	3.58
		High	1.35	0.71	0.89	0.57	0.77	0.66	0.91	0.93	0.84	0.90	5.32
Sump Cut	Blowing	Low	0.93	0.49	0.38	0.58	0.45	0.61	2.57	0.37	0.71	1.18	
		High	1.25	0.82	0.44	0.61	0.73	0.61	3.83	0.59	1.03	1.78	
	Exhausting	Low	0.80	0.71	0.72	0.71	1.29	0.97	1.53	0.74	0.47	0.49	2.28
		High	1.31	1.08	1.08	0.85	2.04	1.38	4.65	2.26	0.96	1.31	4.21

Table 3 summarizes the methane concentration results from all test scenarios. The percent difference from average is the difference between the reading at the machine-mounted sensor location (MMS) and the average of the means of the face readings (FR) Equation 1. A mean was taken for each of the tests run, and an average of the mean values was then taken to show a better representative value than the average of all of the data collected. Because of outliers in the data, the mean was determined to be a more consistent value than the average. The percent difference from maximum is the difference between the reading at the machine-mounted sensor location (MMS) and the maximum face reading (MF) Equation 2. A negative percent difference indicates that the reading at the machine-mounted sensor is lower than the average or maximum.

Equation 1: Percent difference of the Machine Mounted sensor (MMR) from Average Face readings (FR)

$$\text{Percent difference from average} = 1 - \frac{FR}{MMR}$$

Equation 2: Percent different of the Machine Mounted sensor (MMR) from the Maximum face reading (MF)

$$\text{Percent difference from Max} = 1 - \left(\frac{MF}{MMR}\right)$$

Comparing results in

Table 3, only two scenarios show a lower methane measurement at the machine-mounted sensor location than the average face methane: exhausting ventilation, low flow in a slab cut and blowing ventilation, high flow in a sump entry, with differences of 2% and 23%, respectively. All of the other machine-mounted methanometer location readings are higher than the average face readings. This indicates that the machine mounted location for the methane sensor, in these testing scenarios is adequate for determining average methane concentrations at the face with suitable ventilation at the mining face.

When comparing the maximum methane reading on the face to the machine location, only two cases show higher readings at the machine-mounted sensor location than on the face—both were with blowing ventilation. In the other cases, peak face methane readings range from 4% to 52% higher than at the machine-mounted location.

Table 3: Methane concentration for various face ventilation scenarios

Entry Width Cut	Ventilation Setup	Flow	Mean Methanometer reading (machine-mounted sensor location) % CH4	Average face CH4 readings, % CH4	Maximum CH4 face reading % CH4	Percent Difference from Average	Percent Difference from Maximum
Slab Cut	Blowing	Low	0.36	0.25	0.37	30%	-4%
		High	0.38	0.25	0.35	36%	8%
	Exhausting	Low	0.64	0.66	0.98	-2%	-52%
		High	0.47	0.41	0.62	12%	-32%
Sump Cut	Blowing	Low	0.76	0.56	0.70	26%	7%
		High	0.60	0.73	0.86	-23%	-45%
	Exhausting	Low	0.81	0.75	0.95	8%	-18%
		High	0.56	0.55	0.75	1%	-35%

Detailed Analysis of Sump Cut, High flow scenarios

The air flow data for this test scenario was looked at in detail for each location as in Figure 8. The Mean, Median, Mode and statistical information was processed for each test to determine if they were significant. The Median was determined to be a better representation of the velocity data when processed. Variation of the airflow made a Mean or Average less accurate with some outliers in the data. Table 5 shows the air flow magnitude statistical analysis for all three runs for Location 1 for the Sump cut, high flow and blowing ventilation set up test. As we can see, the mean and the median are very close. The outliers cause the mean to be higher than the median. Because of the larger spread of the data, the standard deviation is rather high when compared to the Mean. Additionally the range is large due to the point reading ventilation, which is known to vary. Due to these variations in data and the point reading, it was decided that a Median reading of the ventilation velocity was the most accurate value to use when analyzing data. In Table 5 the break up in the data can be identified and the values that were most frequently recorded by the anemometer in the histogram.

Table 4 is a histogram of the velocity direction in degrees recorded for location 1. Location 1 was a good example of an easily attainable direction with the data. Some

locations like location 4 (Appendix Figure 11) the graphic of the direction degrees shows that the location is between 300-50 degrees, which are within 110 degrees of each other, but in statistical analysis, show a large discrepancy because of the 0-360° nature of direction. With this data for all points, a Mean and Median do not always determine a good value for the data collected.

Table 4: Location one Histogram for velocity directional degrees

<i>Bin</i>	<i>Frequency</i>
60.94525	1
67.01775	0
73.09025	0
79.16274	0
85.23524	3
91.30773	2
97.38023	4
103.4527	7
109.5252	11
115.5977	9
121.6702	16
127.7427	15
133.8152	30
139.8877	23
145.9602	24
152.0327	27
158.1052	42
164.1777	43
170.2502	29
176.3227	61
182.3952	58
188.4677	76
194.5402	103
200.6127	80
206.6852	28
212.7577	7

Table 5: Histogram and statistical break down for airflow magnitude (m/s) for Location 1 of the Sump Cut, High Blow, and Blowing Ventilation test.

<i>Bin</i>	<i>Frequency</i>	<i>Location 1</i>	
0.0232	1		
0.13597	1	Mean	1.24525
0.24874	8	Standard Error	0.01733
0.3615	9	Median	1.22801
0.47427	10	Mode	0.90802
0.58704	14	Standard Deviation	0.4594
0.69981	33	Sample Variance	0.21105
0.81257	47	Kurtosis	0.06244
0.92534	44	Skewness	0.21299
1.03811	57	Range	2.93196
1.15088	86	Minimum	0.0232
1.26365	68	Maximum	2.95516
1.37641	67	Sum	875.412
1.48918	56	Count	703
1.60195	55	Confidence Level(95.0%)	0.03402
1.71472	43		
1.82748	29		
1.94025	19		
2.05302	16		
2.16579	16		
2.27856	13		
2.39132	7		
2.50409	3		

Determining a good value to use when identifying a direction in the airflow values were significantly harder to identify. Again the data varied, and at time to a point where a direction for the ventilation flow could not be determined by the data that was collected and flow was determined to be turbulent at those points (see location 8, Appendix Figure 15). A majority of the location data points did have a direction that could be recorded and identified. As you can see from location 1 data in Figure 12 this location had a consistent directional flow median of 180° (Table 6) which from Figure 10 we can determine the velocity is directed towards the face. When determining the value to be used for air flow direction, the mode was determined to be the best fit value when looking at the graphical data and statistical analysis.

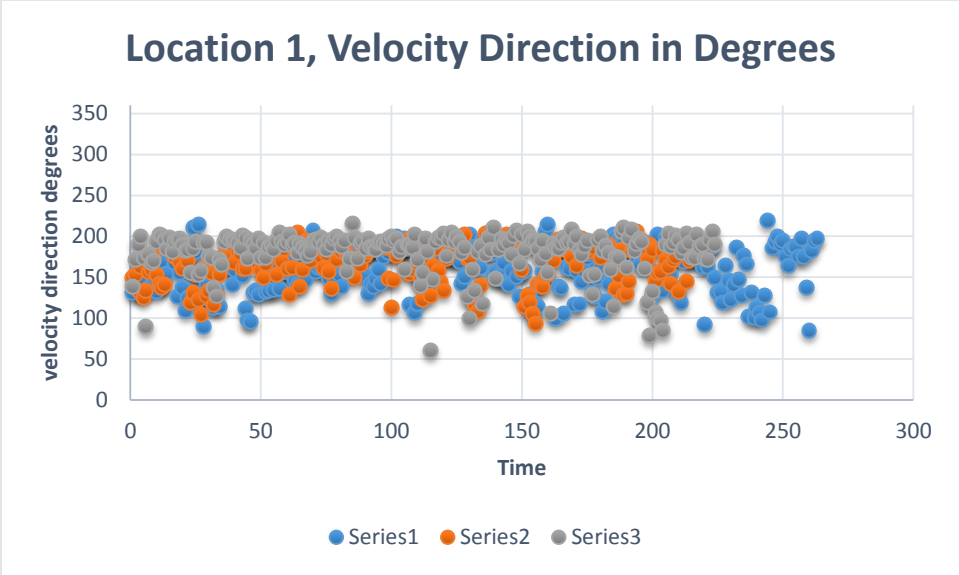


Figure 12: Velocity direction recorded in Degrees for Location 1 of the High flow, Sump Cut, Blowing Ventilation test case. Each series represents a test and the repeats

Table 6 Statistical analysis of Location 1 velocity direction in degrees for the sump cut, high flow, blowing ventilation curtain set up

<i>Location 1 Velocity directional degrees</i>	
Mean	169.200
Standard Error	1.055
Median	176.885
Mode	180.000
Standard Deviation	27.983
Sample Variance	783.035
Kurtosis	0.194
Skewness	-0.912
Range	157.885
Minimum	60.945
Maximum	218.830
Sum	118947.708
Count	703.000
Confidence Level(95.0%)	2.072

Using the Median air flow velocity and the Mode of the air flow directional degrees in **Table 7** an AutoCAD drawing of the flow patterns for this data was created. Figure 13 shows this information graphically for this test case. Using the Mode for velocity

direction to get the direction of the airflow in Figure 13, but it was determined for location 8, that the air is turbulent and a direction will not properly determine the direction of the airflow over time in one direction (Appendix Figure 15). But for visual purposes, the Mode was selected for this point.

Table 7: Mean, Median, Mode and Standard Deviation for each location air flow velocity and directional degrees for the High flow, Sump cut, Blowing ventilation case

Air flow Velocity in m/s										
Location	1	2	3	4	5	6	7	8	9	10
Mean	1.24	0.82	0.44	0.61	0.73	0.61	3.82	0.59	1.04	1.78
Median	1.23	0.72	0.37	0.62	0.75	0.58	3.86	0.51	0.98	1.81
Mode	0.91	0.62	0.18	0.40	0.53	1.31	3.85	0.17	0.57	1.60
Standard Deviation	0.46	0.54	0.32	0.22	0.27	0.34	0.23	0.40	0.57	0.68
Air flow directional degree										
Location	1	2	3	4	5	6	7	8	9	10
Mean	169.2	117.8	157.6	215.5	66.6	108.6	179.9	216.0	211.5	201.4
Median	176.9	54.4	117.1	330.0	26.6	81.76	181.2	220.0	207.5	199.2
Mode	180.0	45.4	90.0	346.0	360.0	30.0	182.2	330.0	178.5	221.0
Standard Deviation	27.9	114.4	86.2	159.5	103.9	96.8	6.0	106.4	48.2	30.0

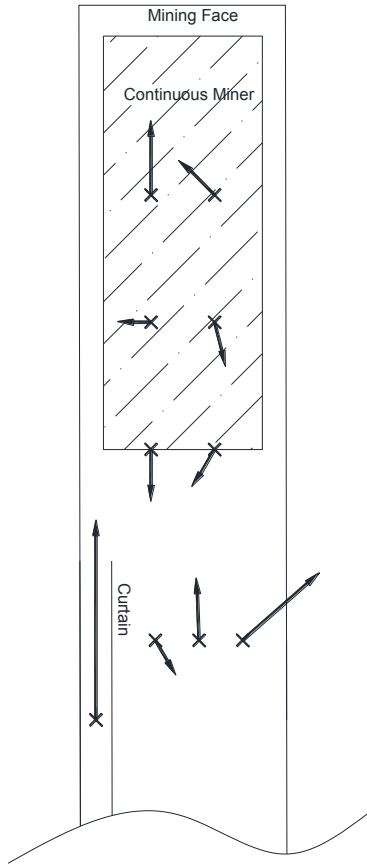


Figure 13: A figure showing air velocity direction, the arrow indicates magnitude. NTS

Discussion

In the sump or first cut, the highest methane readings were in the right corner of the cut, indicating that even with the sprays directing air, they also push the methane across the face, which builds up in the right corner. Previous empty-entry monitoring in the ventilation gallery and with CFD modeling (Wala, Vytla et al. 2007, Taylor, Chilton et al. 2010) showed that airflow in a sump cut entry creates a “figure 8” airflow pattern, and higher methane readings were found in the left corner of the entry. Methane data developed in this research (

Table 3) suggests a different airflow pattern at the face from the previous empty-entry ventilation flow work, most likely due to the presence of the CM machine at the face and the use of water sprays and scrubber fan. A more U-shaped airflow pattern across the face is evident. In the slab or second cut entry, a lower methane concentration was shown in the right corner of the face—a result different from the work done in previous laboratory and CFD modeling in an empty entry (Taylor et al. 2010), which showed the highest face methane concentrations at that location. This also suggests that with the CM at the face, scrubber and water sprays largely affect the flow of the air within the face area in comparison to modeling without these parameters.

In all cases, ventilation velocity on the left side (Location 1 from Figure 8) of the CM was higher than on the right. This indicates that pushing the air from left to right across the face is significant enough to be seen 3.6 m (12 ft) from the face. This is significant because regardless of whether the air is being directed by a blowing curtain or an exhausting curtain, the left to right airflow is consistent.

As in previous research (Schlick and Dalzell 1963, Dalzell 1966), tests supported the conclusion that blowing curtain ventilation was more efficient in moving fresh air to the face and sweeping away methane than exhausting curtain ventilation. This same result is shown in this research by lower methane readings shown in the blowing curtain setup by comparison to the exhaust curtain setup (Table 3). An exception was in the high flow ventilation case for the slab cut, where methane values were higher in the blowing curtain case than the exhausting, possibly due to the higher air velocity in the smaller entry causing more turbulence, resulting in less effective airflow to dilute and remove methane. A more thorough analysis of airflow, possibly via a CFD program, would detail why this situation occurs.

Only one case showed average face methane readings to be significantly higher than with the machine-mounted methanometer. The blowing ventilation, high flow, sump cut entry test case showed an average face methane concentration of 0.73%, which was 23% higher than the machine-mounted methanometer reading of 0.60%. All other cases showed methane readings close to or higher at the machine methanometer than

face location averages, indicating effective placement of the machine-mounted methanometer when compared to actual average face readings.

Comparing maximum face methane readings to actual machine-mounted sensor readings, only two maximums fell below the reading at the machine sensor. The face maximum ranged from 4% to 52% higher than at the machine-mounted methanometer, indicating that when the machine sensor methane readings are 2.0%, face locations could have a methane concentration 50% higher than at the machine mounted methanometer, or over 3.0%. These values show that under these test conditions, a 2% methane reading at the monitor would have shut off equipment power well below the 5% lower explosive limit.

Chapter 5: Conclusions and Recommendations

Full-scale testing for examining distributions of airflow and methane concentration was conducted in a deep cut continuous miner face simulator using blowing and exhausting ventilation. Technologies such as ultrasonic anemometers allows digital recording of ventilation patterns in and around the face in the laboratory environment provides a significant opportunity to expand research knowledge of ventilation flow around the critical mining face area. The deep cut face has the lowest airflow quantity to the face, is furthest away from the auxiliary ventilation, and has the highest potential for a methane buildup at the face.

Laboratory testing allow us to regulate inputs to better understand what each variable controls allowing better understanding of their effects. It also allows us to collect detailed information for use in verifying highly detailed CFD model for a CM face. Some variables that are not tested in the laboratory need to be taken into consideration when applying these results in an underground mine. An example of a variable seen underground that would not be considered in the laboratory is a plugged or partially plugged scrubber filter. These issues need to be taken into consideration when applying to a coal mine setting.

Based on the analysis of two different entry widths or cut sequences, it is found that the highest methane reading is in the right corner of the narrower entry or sump cuts. This indicates an airflow path which travels directly up the left side of the mining machine and across the face from left to right. Corners of the mining entry are the hardest area of the face to ventilate effectively, and have the greatest likelihood of accumulating contaminants. In this testing, the slab cut ventilation flow shows that lower face methane readings were consistently in the right corner. This indicates that this corner is getting more fresh air than in the sump cut case, with the slab cut entry possibly encouraging a “figure 8” airflow pattern above the miner as shown in previous CFD modeling (Wala, Vytla et al. 2007, Taylor, Chilton et al. 2010).

This work confirms previous laboratory research that blowing curtain ventilation is more efficient at moving fresh air to the face than exhaust curtain ventilation even with the CM machine at the face. There was an exception in the high flow ventilation case for the

sump cut entry, where methane values were higher in the blowing curtain case than the exhausting case. The blowing ventilation, high flow, sump cut entry case shows that the average face methane concentration was much higher than the mean machine-mounted methanometer reading.

More work should be done to examine face ventilation with the CM in place and incorporate other factors such as variations in scrubbers and sprays. These issues have been studied separately, but never combined with CFD computer modeling and full-scale testing for verification and validation. Information can be gathered and used to validate highly detailed CFD modeling for airflow in a deep cut scenario, a critical challenge for ventilation engineers.

Future work is recommended to better explain the airflow around mining machine obstructions in the face and the effect of the water sprays and scrubber flow. Goodman and Taylor (Goodman and Taylor 1993, Taylor and Goodman 1997) concluded that the methane concentration error at the machine-mounted methane sensor was influenced primarily by the location of the mining machine at the face. These laboratory tests do not take into consideration issues such as operators standing in front of a blowing curtain, positioning of operators, other operating equipment in the entry, or crosscut ventilation. Limitations of the ventilation gallery and monitoring equipment are that they give a basic understanding of a more detailed ventilation scheme and methane dilution in a static laboratory setting.

References:

CFR (2011). Code of Federal Regulations. O. o. t. F. Register. Washington, DC, U.S. Government Printing office. **30**.

Colinet, J., J. M. Listak, J. A. Organiscak, J. P. Rider and A. L. Wolfe (2010). Best practices for dust control in coal mining, Department of Health and Human Services, Centers for Disease Control and Prevention, National Institute for Occupational Safety and Health, Office of Mine Safety and Health Research.

Dalzell, R. W. (1966). Face ventilation in underground bituminous coal mines, performance characteristics of common jute line brattice, Bureau of Mines, Washington, DC (USA).

Goodman, G. V. and C. D. Taylor (1993). "Effectiveness of methane monitoring for estimating face gas conditions during deep cutting." Journal of the Mine Ventilation Society of South Africa **46**(6): 86-92.

Hall, E., C. Taylor and J. Chilton (2007). Using ultrasonic anemometers to evaluate face ventilation conditions. Proceedings of the SME Annual Meeting and Exhibit.

Hargreaves, D. M. and I. S. Lowndes (2007). "The computational modeling of the ventilation flows within a rapid development drivage." Tunnelling and Underground Space Technology **22**(2): 150-160.

Kissell, F. (1979). "Improved face ventilation by spray jet systems." Second Annual Mining Institute, University of Alabama.

Kissell, F. N. (2003). "Dust control methods in tunnels and underground mines." Handbook for dust control in mining. Pittsburgh, PA: US Department of Health and Human Services, Centers for Disease Control and Prevention, National Institute for Occupational Safety and Health, DHHS (NIOSH) Publication(2003-147): 3-21.

Kissell, F. N., J. Banfield Jr, R. Dalzell and M. Zabetakis (1974). Peak Methane Concentrations During Coal Mining: An Analysis, US Bureau of Mines.

Martikainen, A., H. Dougherty, C. Taylor and A. Mazzella (2010). Sonic anemometer airflow monitoring technique for use in underground mines. Proceedings of the 13th US/North American Mine Ventilation Symposium.

Martikainen, A., C. Taylor and A. Mazzella (2011). Effects of obstructions, sample size and sample rate on ultrasonic anemometer measurements underground. SME Annual Meeting, Pre-Print.

Matta, J. E. (1976). Effect of location and type of water sprays for respirable dust suppression on a continuous-mining machine, US Dept. of the Interior, Bureau of Mines.

Petrov, T. and A. Wala (2014). Improvement of blowing curtain face ventilation systems using passive regulator. SME Annual Meeting, Salt Lake City, Utah, SME.

Schlick, D. P. and R. W. Dalzell (1963). Ventilation of continuous-miner places in coal mines, Bureau of Mines, Washington, DC (USA).

Stahl, R. W. (1958). Auxiliary ventilation of continuous miner places, Bureau of Mines, Washington, DC (USA).

Taylor, C., J. Chilton and G. Goodman (2010). "Guidelines for the Control and Monitoring of Methane Gas on Continuous Mining Operations." DHHS (NIOSH) Publication(2010-141): 1-75.

Taylor, C., J. Chilton and T. Mal (2002). Evaluating performance characteristics of machine-mounted methane monitors by measuring response time. Proc. 9th US Mine Vent Symp.

Taylor, C., J. Chilton and T. Mal (2002). Evaluating performance characteristics of machine-mounted methane monitors by measuring response time. Proceedings, 9th US/NA Mine Ventilation Symposium, Queens University, Kingston, ON, Canada, June 8-12, Lisse, AA Balkema.

Taylor, C., R. Timko, M. Senk and A. Lusin (2004). "Measurement of airflow in a simulated underground mine environment using an ultrasonic anemometer." TRANSACTIONS-SOCIETY FOR MINING METALLURGY AND EXPLORATION INCORPORATED **316**: 201.

Taylor, C. D. and G. V. Goodman (1997). "Use of methane monitors for estimating face gas conditions." Applied occupational and environmental hygiene **12**(12): 947-951.

Taylor, C. D., R. J. Timko, E. D. Thimons and T. Mal (2007). "Using ultrasonic anemometers to evaluate factors affecting face ventilation effectiveness." TRANSACTIONS-SOCIETY FOR MINING METALLURGY AND EXPLORATION INCORPORATED **320**: 127.

Thimons, E. D., C. D. Taylor and J. A. Zimmer (1999). "Ventilating the box cut of a two-pass 40 ft extended cut." Journal of the Mine Ventilation Society of South Africa **52**(3): 108-115.

Unwin, I. D. (November 2007). The Measurement of Air Flow
in British Coal Mines: A

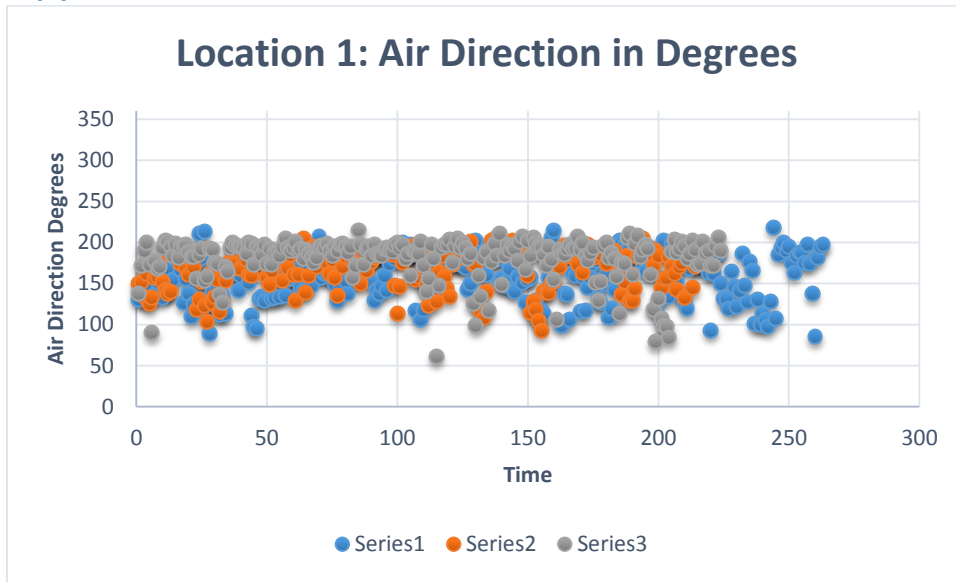
Historical Review. http://www.cmhrc.co.uk/cms/document/air_flow_2007.pdf, The Coalmining History Resource Centre: 88.

Volkwein, J. and E. Thimons (1986). Extended advance of continuous miner successfully ventilated with a scrubber in a blowing section, Society of Mining Engineers of AIME, Littleton, CO.

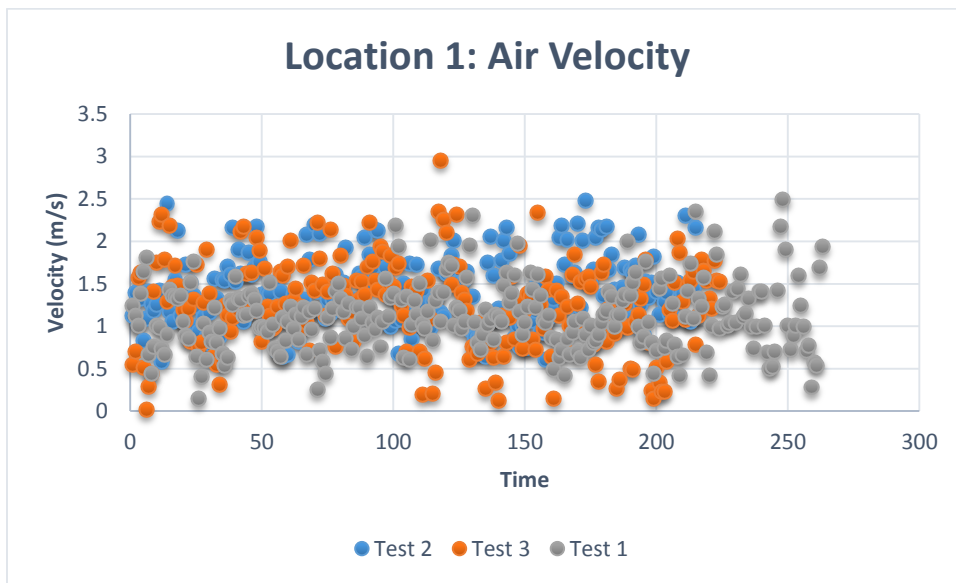
Wala, A., V. S, H. G and C. Taylor (2008). Study on the effects of scrubber operation on the face ventilation. 12th U.S./North American Mine Ventilation Symposium. K. Wallace Jr, SME: 281-286.

Wala, A., S. Vytla, C. Taylor and G. Huang (2007). "Mine face ventilation: a comparison of CFD results against benchmark experiments for the CFD code validation." Mining Engineering **59**(10): 49-55.

Appendix A



Appendix Figure 1: Graphical data of Velocity direction in degrees over time for the three different repeat tests run



Appendix Figure 2: Graphical data of air velocity magnitude (m/s) over time for the three repeat tests run

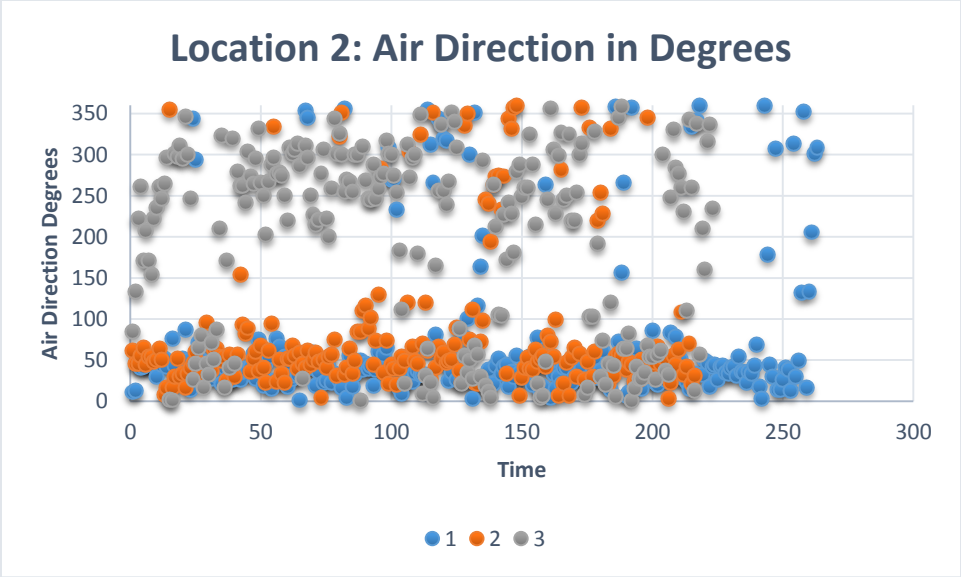
<i>Location 1 Degrees</i>		<i>Location 1 Velocity</i>	
Mean	169.2002	Mean	1.245251
Standard Error	1.05539	Standard Error	0.017327
Median	176.8845	Median	1.228007
Mode	180.0004	Mode	0.90802
Standard Deviation	27.98276	Standard Deviation	0.459405
Sample Variance	783.0347	Sample Variance	0.211053
Kurtosis	0.193931	Kurtosis	0.062441
Skewness	-0.91204	Skewness	0.212987
Range	157.8849	Range	2.931962
Minimum	60.94525	Minimum	0.0232
Maximum	218.8302	Maximum	2.955162
Sum	118947.7	Sum	875.4115
Count	703	Count	703
Confidence Level(95.0%)	2.072098	Confidence Level(95.0%)	0.034019

Appendix Table 1: Statistical breakdown of Location 1, air flow Directional Degrees and velocity

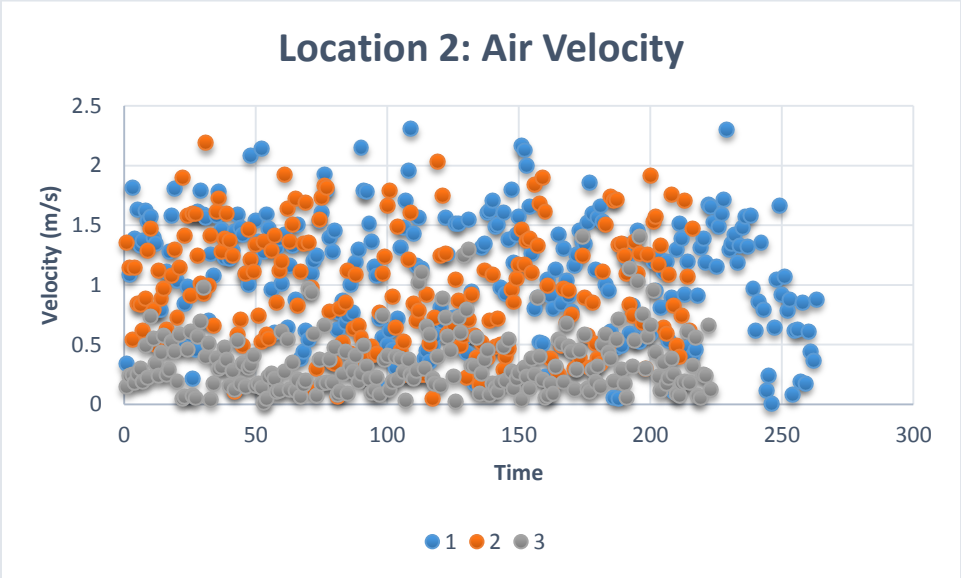
Location 1 Velocity		Location 1 Degrees	
<i>Bin</i>	<i>Frequency</i>	<i>Bin</i>	<i>Frequency</i>
0.0232	1	60.94525	1
0.135968	1	67.01775	0
0.248736	8	73.09025	0
0.361503	9	79.16274	0
0.474271	10	85.23524	3
0.587039	14	91.30773	2
0.699807	33	97.38023	4
0.812575	47	103.4527	7
0.925342	44	109.5252	11
1.03811	57	115.5977	9
1.150878	86	121.6702	16
1.263646	68	127.7427	15
1.376413	67	133.8152	30
1.489181	56	139.8877	23
1.601949	55	145.9602	24
1.714717	43	152.0327	27
1.827485	29	158.1052	42
1.940252	19	164.1777	43
2.05302	16	170.2502	29
2.165788	16	176.3227	61
2.278556	13	182.3952	58
2.391324	7	188.4677	76
2.504091	3	194.5402	103
2.616859	0	200.6127	80
2.729627	0	206.6852	28
2.842395	0	212.7577	7

Appendix Table 2: Histogram of Location 1, air flow directional degrees (in 0-360 degrees) and velocity (in m/s)

Location 2:



Appendix Figure 3: Graphical data of air velocity direction in degrees over time for the three test repeats



Appendix Figure 4: Graphical data of air velocity magnitude (m/s) over time for the three test repeats

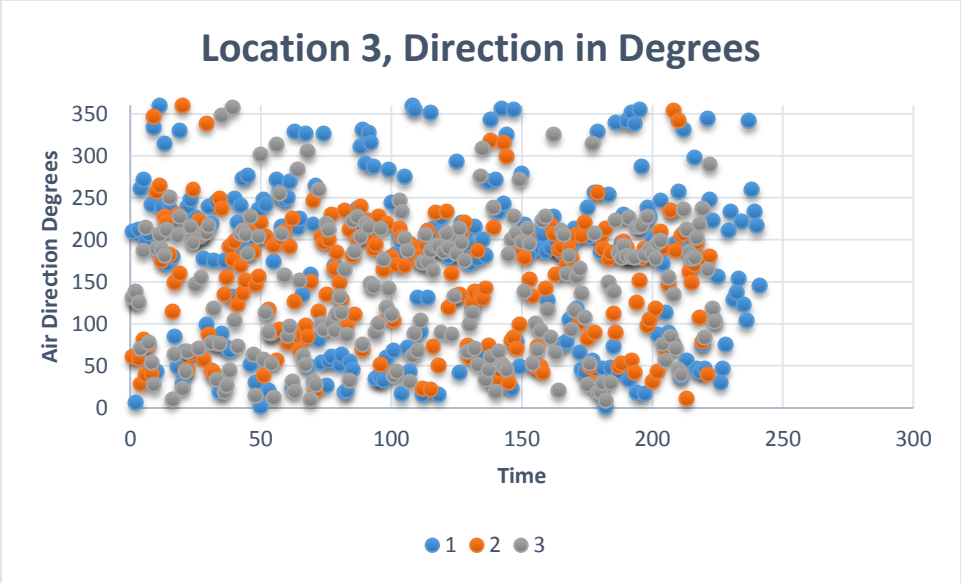
<i>Location 2 Directional Degrees</i>		<i>Location 2 Air Velocity</i>	
Mean	117.8189493	Mean	0.821566
Standard Error	4.182717836	Standard Error	0.020281
Median	54.40384901	Median	0.718503
Mode	45.37618096	Mode	0.618466
Standard Deviation	114.4720544	Standard Deviation	0.537354
Sample Variance	13103.85124	Sample Variance	0.28875
	-		
Kurtosis	0.846723373	Kurtosis	-0.8916
Skewness	0.903064494	Skewness	0.40694
Range	358.9533021	Range	2.298679
Minimum	0.945405258	Minimum	0.01
Maximum	359.8987073	Maximum	2.308679
Sum	88246.39301	Sum	576.7391
Count	749	Count	702
Confidence		Confidence	
Level(95.0%)	8.211262871	Level(95.0%)	0.039819

Appendix Table 3: Statistical breakdown of Location 2, air flow directional degrees and velocity

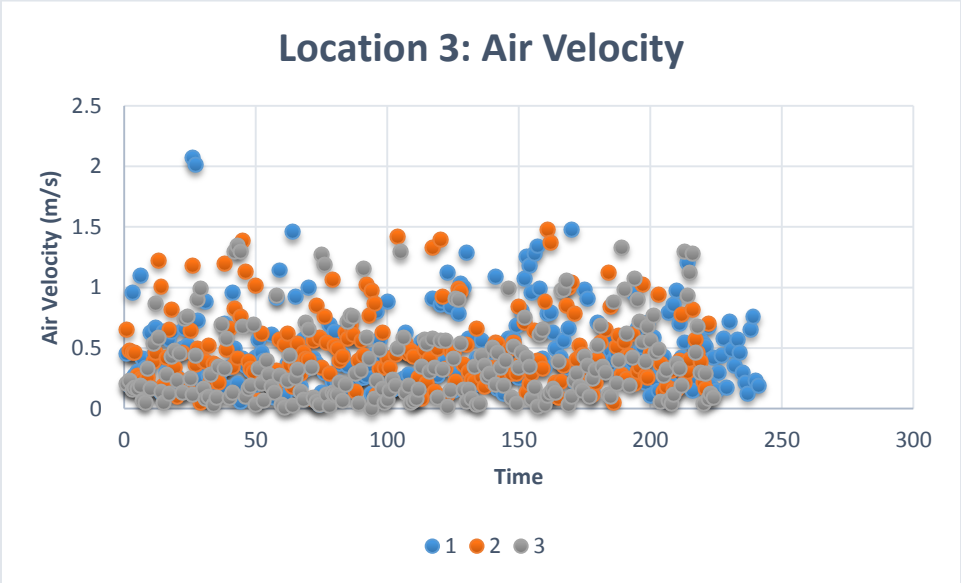
Location 2 Velocity		Location 2 Direction	
<i>Bin</i>	<i>Frequency</i>	<i>Bin</i>	<i>Frequency</i>
0.01	1	0.945405	1
0.098411	30	14.23997	35
0.186821	51	27.53454	94
0.275232	55	40.82911	111
0.363643	40	54.12367	131
0.452053	46	67.41824	74
0.540464	46	80.71281	26
0.628875	52	94.00737	16
0.717286	30	107.3019	11
0.805696	30	120.5965	12
0.894107	26	133.8911	4
0.982518	29	147.1856	0
1.070929	18	160.4802	5
1.159339	33	173.7748	6
1.24775	29	187.0693	4
1.336161	33	200.3639	4
1.424572	36	213.6585	8
1.512982	26	226.953	10
1.601393	31	240.2476	13
1.689804	19	253.5422	18
1.778214	12	266.8367	27
1.866625	13	280.1313	23
1.955036	5	293.4259	10
2.043447	3	306.7204	28
2.131857	2	320.015	19
2.220268	4	333.3096	15
		346.6041	22

Appendix Table 4: Histogram of Location 2, air flow directional degrees and velocity (m/s)

Location 3:



Appendix Figure 5: Graphical data of air velocity direction in degrees over time for the three test repeats



Appendix Figure 6: Graphical data of air velocity magnitude (m/s) over time for three test repeats

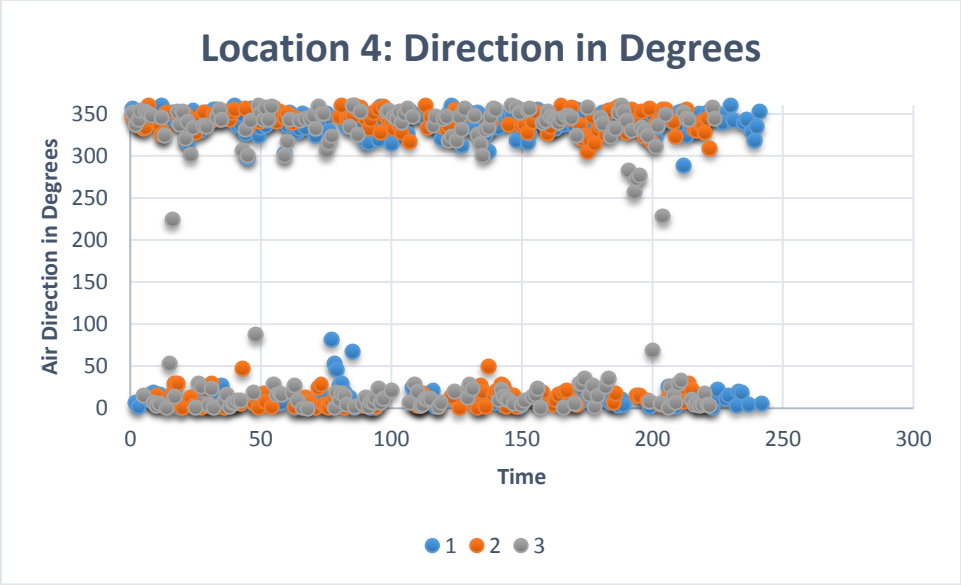
<i>Location 3 Air Velocity</i>		<i>Location 3 Directional Degree</i>	
Mean	0.445707	Mean	157.5965
Standard Error	0.012255	Standard Error	3.290584
Median	0.37	Median	177.1372
Mode	0.180278	Mode	89.99979
Standard Deviation	0.321217	Standard Deviation	86.24847
Sample Variance	0.10318	Sample Variance	7438.798
Kurtosis	2.061882	Kurtosis	-0.7093
Skewness	1.312222	Skewness	0.138551
Range	2.068469	Range	358.6361
Minimum	0.0024	Minimum	1.363924
Maximum	2.070869	Maximum	360
Sum	306.2009	Sum	108268.8
Count	687	Count	687
Confidence Level(95.0%)	0.024062	Confidence Level(95.0%)	6.460826

Appendix Table 5: Statistical breakdown of Location 3, air flow directional degrees and velocity

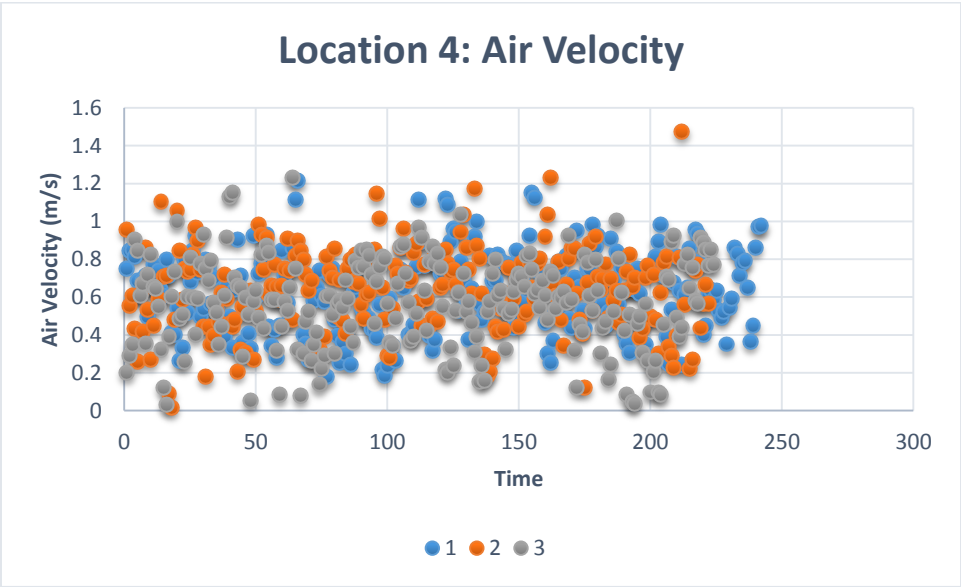
Location 3 Velocity		Location 3 Direction	
<i>Bin</i>	<i>Frequency</i>	<i>Bin</i>	<i>Frequency</i>
0.0024	1	1.363924	1
0.081957	40	15.15762	8
0.161513	76	28.95131	28
0.24107	93	42.74501	32
0.320626	79	56.53871	48
0.400183	87	70.3324	32
0.479739	67	84.1261	35
0.559296	50	97.91979	28
0.638852	47	111.7135	25
0.718409	33	125.5072	20
0.797965	19	139.3009	29
0.877522	14	153.0946	17
0.957078	18	166.8883	21
1.036635	22	180.682	36
1.116191	7	194.4757	63
1.195748	9	208.2694	70
1.275304	5	222.063	53
1.354861	11	235.8567	37
1.434417	4	249.6504	27
1.513974	3	263.4441	13
1.59353	0	277.2378	12
1.673087	0	291.0315	7
1.752643	0	304.8252	4
1.8322	0	318.6189	9
1.911756	0	332.4126	10
1.991313	0	346.2063	9
More	2	More	13

Appendix Table 6: Histogram of Location 3, air flow directional degrees and velocity (m/s)

Location 4:



Appendix Figure 7: Graphical data of velocity direction in degrees over time for the three test repeats



Appendix Figure 8: Graphical data of air velocity magnitude (m/s) over time for the three test repeats

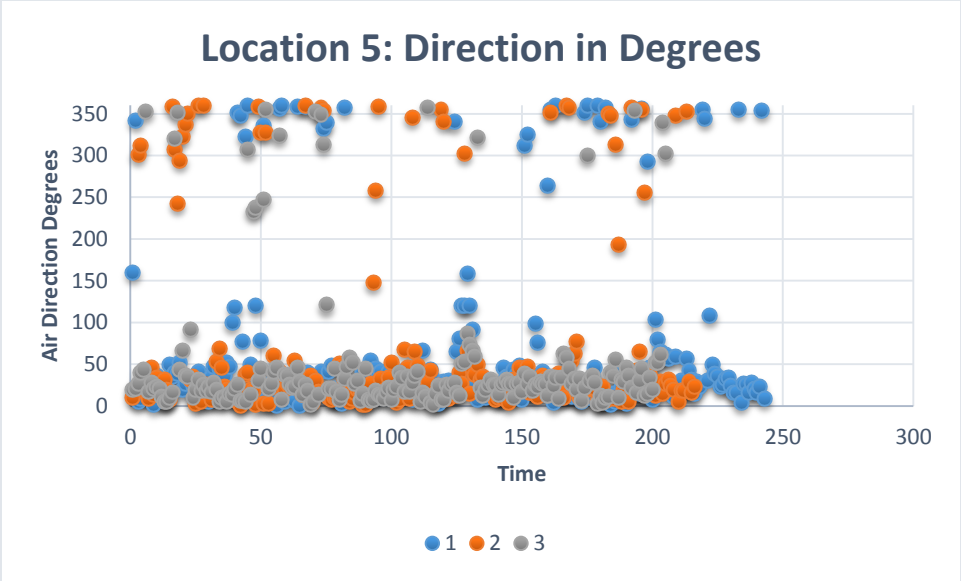
<i>Location 4 Air Velocity</i>		<i>Location 4 Directional Degree</i>	
Mean	0.608751	Mean	215.4974
Standard Error	0.008609	Standard Error	6.080095
Median	0.619314	Median	330.9947
Mode	0.403113	Mode	346.0051
Standard Deviation	0.225807	Standard Deviation	159.4794
Sample Variance	0.050989	Sample Variance	25433.68
Kurtosis	0.023702	Kurtosis	-1.74427
Skewness	-0.03061	Skewness	-0.48055
Range	1.456279	Range	359.8804
Minimum	0.02	Minimum	0.018324
Maximum	1.476279	Maximum	359.8987
Sum	418.8209	Sum	148262.2
Count	688	Count	688
Confidence Level(95.0%)	0.016903	Confidence Level(95.0%)	11.9378

Appendix Table 7: Statistical breakdown of Location 4 air flow directional degrees and velocity

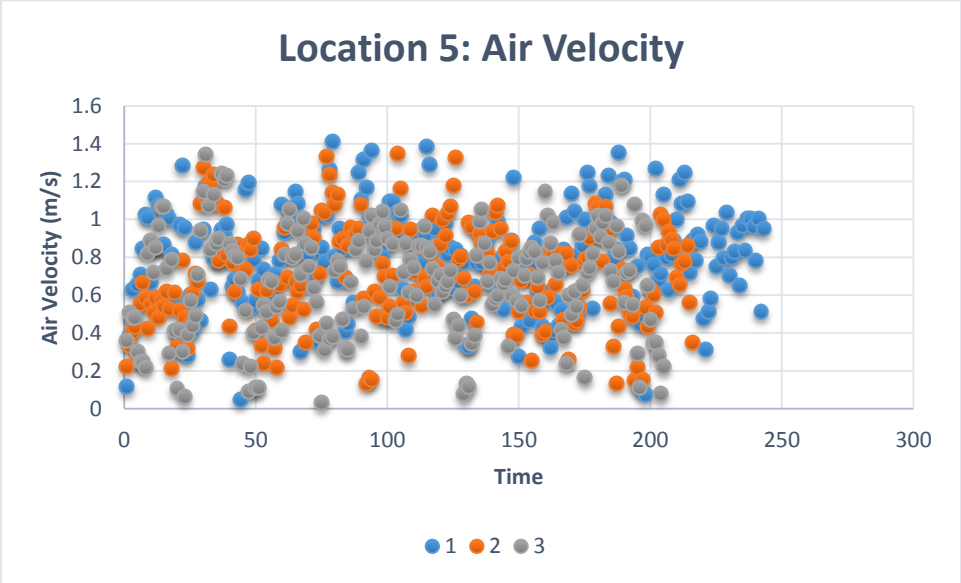
Location 4 Velocity		Location 4 Direction	
<i>Bin</i>	<i>Frequency</i>	<i>Bin</i>	<i>Frequency</i>
0.02	1	0.018324	1
0.076011	4	13.85988	162
0.132022	10	27.70143	73
0.188033	8	41.54298	17
0.244043	15	55.38454	5
0.300054	30	69.22609	2
0.356065	35	83.06764	1
0.412076	33	96.9092	1
0.468086	47	110.7507	0
0.524097	55	124.5923	0
0.580108	56	138.4339	0
0.636118	74	152.2754	0
0.692129	61	166.117	0
0.74814	63	179.9585	0
0.804151	67	193.8001	0
0.860161	51	207.6416	0
0.916172	27	221.4832	0
0.972183	24	235.3247	2
1.028193	8	249.1663	0
1.084204	4	263.0078	1
1.140215	7	276.8494	1
1.196226	4	290.6909	3
1.252236	3	304.5325	6
1.308247	0	318.374	20
1.364258	0	332.2156	55
1.420269	0	346.0572	164
More	1	More	174

Appendix Table 8: Histogram of Location 4 air flow directional degrees and velocity (m/s)

Location 5:



Appendix Figure 9: Graphical data of velocity direction in degrees over time for the three test repeats



Appendix Figure 10: Graphical data of air velocity magnitude (m/s) over time for the three test repeats

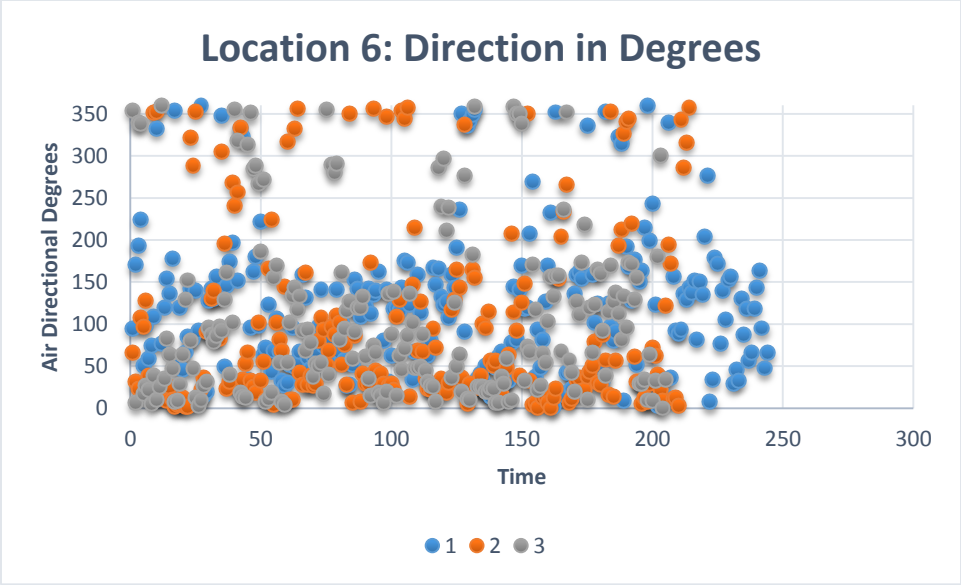
<i>Location 5 Air Velocity</i>		<i>Location 5 Directional Degree</i>	
Mean	0.730029	Mean	66.6029
Standard Error	0.010635	Standard Error	4.03408
Median	0.753724	Median	26.56499
Mode	0.533385	Mode	360
Standard Deviation	0.274036	Standard Deviation	103.951
Sample Variance	0.075096	Sample Variance	10805.8
Kurtosis	-0.33162	Kurtosis	2.968152
Skewness	-0.17307	Skewness	2.154056
Range	1.380174	Range	359.5018
Minimum	0.032129	Minimum	0.49821
Maximum	1.412303	Maximum	360
Sum	484.7392	Sum	44224.32
Count	664	Count	664
Confidence Level(95.0%)	0.020882	Confidence Level(95.0%)	7.921112

Appendix Table 9: Statistical breakdown of location 5 air flow directional degrees and velocity

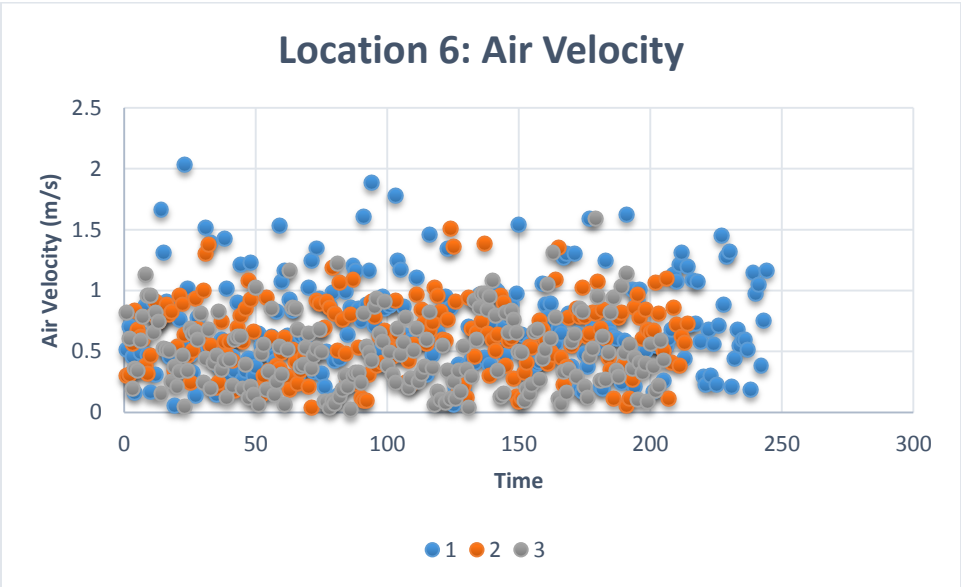
Location 5 Velocity		Locaiton 5 Degree	
<i>Bin</i>	<i>Frequency</i>	<i>Bin</i>	<i>Frequency</i>
0.032129	1	0.49821	1
0.087336	5	14.87828	152
0.142543	11	29.25835	215
0.19775	5	43.63843	119
0.252957	12	58.0185	52
0.308164	13	72.39857	18
0.363371	21	86.77864	7
0.418577	26	101.1587	5
0.473784	28	115.5388	2
0.528991	36	129.9189	6
0.584198	40	144.2989	0
0.639405	42	158.679	1
0.694612	47	173.0591	2
0.749819	40	187.4391	0
0.805026	54	201.8192	1
0.860233	63	216.1993	0
0.91544	48	230.5794	0
0.970647	46	244.9594	3
1.025854	40	259.3395	3
1.081061	28	273.7196	1
1.136268	15	288.0996	0
1.191475	14	302.4797	6
1.246682	12	316.8598	6
1.301889	8	331.2399	8
1.357096	6	345.6199	12
More	3	More	44

Appendix Table 10: Histogram of location 5 air flow directional degrees and velocity (m/s)

Location 6:



Appendix Figure 11: Graphical data of velocity direction in degrees over time for the three test repeats



Appendix Figure 12: Graphical data of air velocity magnitude (m/s) over time for the three test repeats

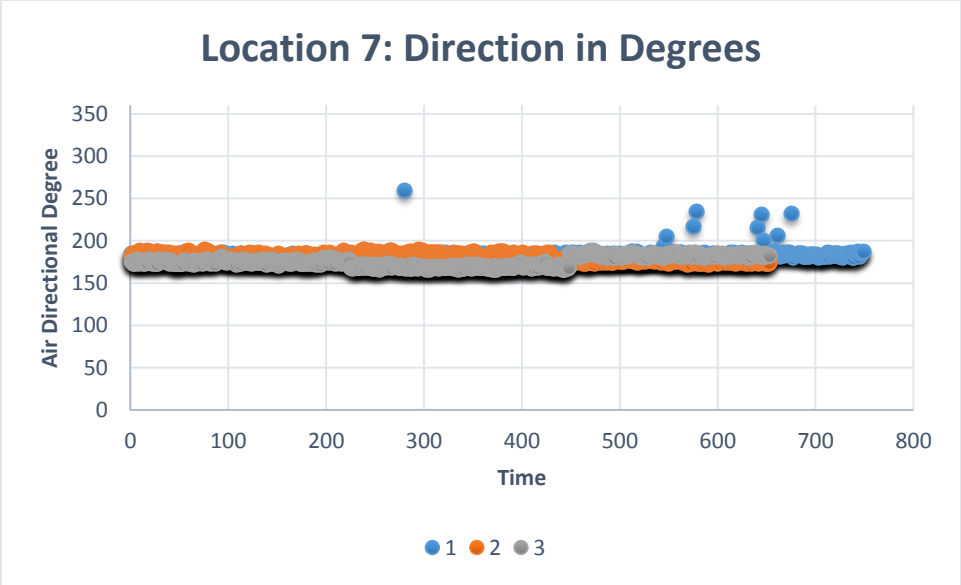
<i>Location 6 Air Velocity</i>		<i>Location 6 Directional Degree</i>	
Mean	0.610238	Mean	108.6295
Standard Error	0.013172	Standard Error	3.758882
Median	0.585154	Median	81.76592
Mode	1.313202	Mode	29.99994
Standard Deviation	0.339156	Standard Deviation	96.78664
Sample Variance	0.115027	Sample Variance	9367.654
Kurtosis	0.684678	Kurtosis	0.659812
Skewness	0.735375	Skewness	1.213089
Range	2.013615	Range	359.74
Minimum	0.019756	Minimum	0.25513
Maximum	2.033372	Maximum	359.9951
Sum	404.5877	Sum	72021.38
Count	663	Count	663
Confidence Level(95.0%)	0.025863	Confidence Level(95.0%)	7.380767

Appendix Table 11: Statistical breakdown of location 6 air flow directional degrees and velocity

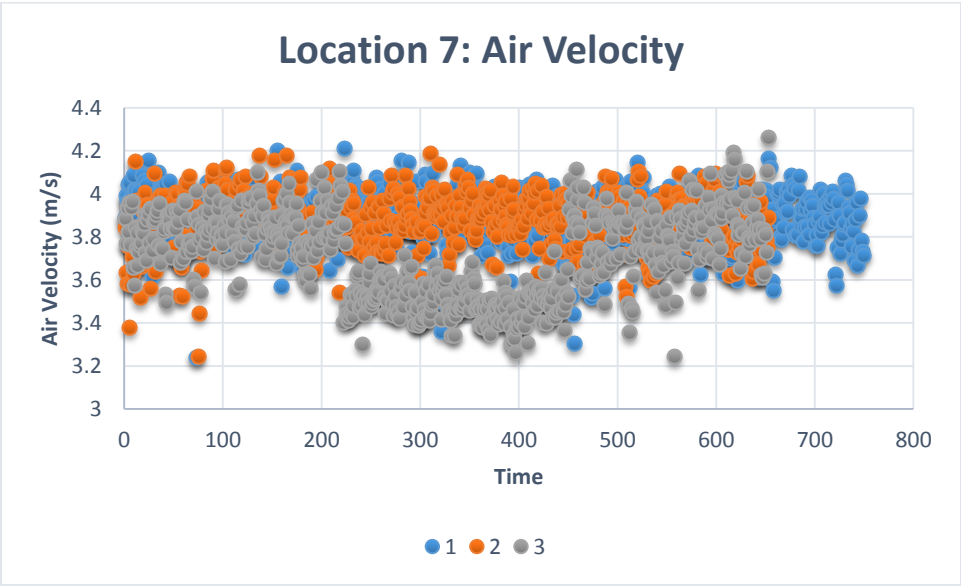
Location 6 Velocity		Location 6 Degree	
<i>Bin</i>	<i>Frequency</i>	<i>Bin</i>	<i>Frequency</i>
0.019756	1	0.25513	1
0.100301	20	14.64473	67
0.180846	37	29.03433	73
0.261139	51	43.42393	76
0.341935	46	57.81353	48
0.422479	55	72.20313	47
0.503024	57	86.59272	29
0.583569	64	100.9823	42
0.664113	78	115.3719	23
0.744658	45	129.7615	45
0.825202	46	144.1511	38
0.905747	44	158.5407	28
0.986292	39	172.9303	29
1.066836	17	187.3199	13
1.147381	15	201.7095	8
1.227925	13	216.0991	8
1.30847	9	230.4887	5
1.389015	10	244.8783	8
1.469559	4	259.2679	1
1.550104	4	273.6575	5
1.630648	4	288.0471	6
1.711193	1	302.4367	6
1.791738	1	316.8263	4
1.872282	0	331.2159	6
1.952827	1	345.6055	16
More	1	More	31

Appendix Table 12: Histogram of location 6 air flow directional degrees and velocity (m/s)

Location 7: (Blowing Curtain Location)



Appendix Figure 13: Graphical data of velocity direction in degrees over time for the three test repeats



Appendix Figure 14: Graphical data of air velocity magnitude (m/s) over time for the three test repeats

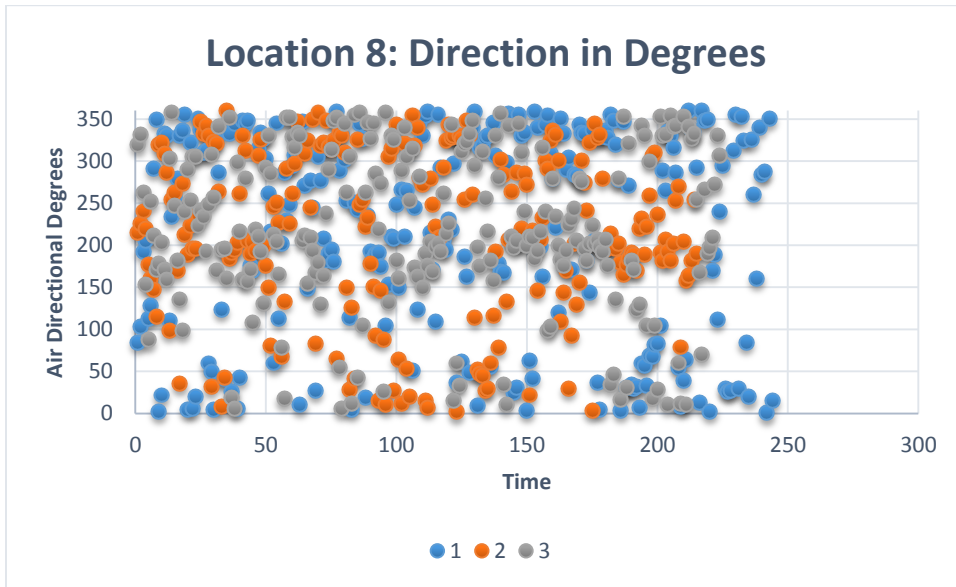
<i>Location 7 Velocity</i>		<i>Location 7 Degrees</i>	
Mean	3.816984	Mean	179.9377
Standard Error	0.005092	Standard Error	0.132789
Median	3.858108	Median	181.1822
Mode	3.850987	Mode	182.1635
Standard Deviation	0.230819	Standard Deviation	6.019615
Sample Variance	0.053277	Sample Variance	36.23577
Kurtosis	52.70936	Kurtosis	23.98187
Skewness	-5.03311	Skewness	1.834123
Range	3.879026	Range	94.1658
Minimum	0.382753	Minimum	165.6896
Maximum	4.261779	Maximum	259.8554
Sum	7843.901	Sum	369771.9
Count	2055	Count	2055
Confidence Level(95.0%)	0.009986	Confidence Level(95.0%)	0.260416

Appendix Table 13: Statistical breakdown of location 7 air flow directional degrees and velocity

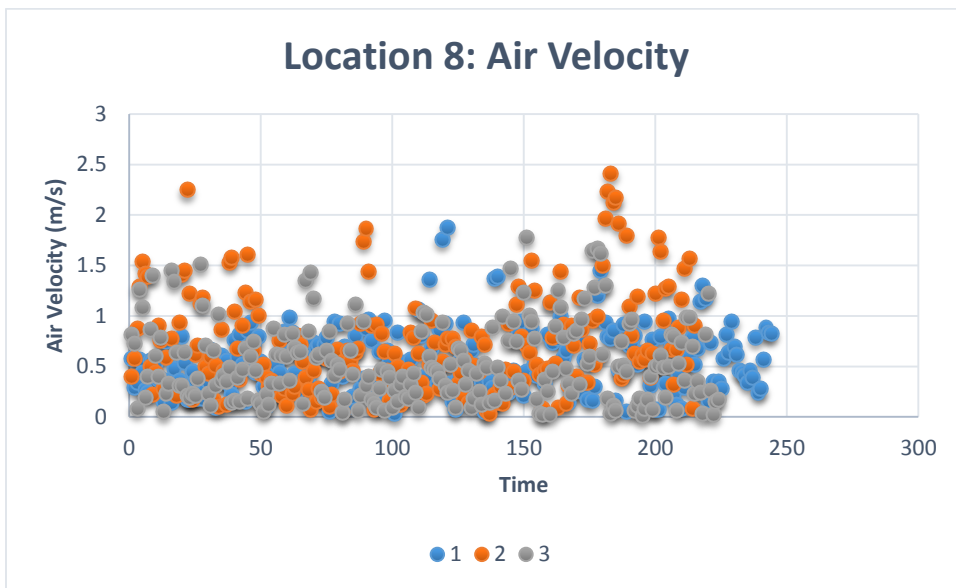
Location 7 Velocity		Locaiton 7 Degrees	
<i>Bin</i>	<i>Frequency</i>	<i>Bin</i>	<i>Frequency</i>
0.382753	1	165.6896	1
0.468954	0	167.7822	24
0.555154	0	169.8747	136
0.641355	0	171.9673	57
0.727555	0	174.0599	97
0.813756	0	176.1525	176
0.899957	0	178.245	161
0.986157	0	180.3376	202
1.072358	0	182.4302	501
1.158558	1	184.5228	334
1.244759	1	186.6153	294
1.33096	0	188.7079	54
1.41716	0	190.8005	8
1.503361	0	192.8931	0
1.589561	0	194.9856	1
1.675762	0	197.0782	0
1.761962	1	199.1708	0
1.848163	0	201.2633	1
1.934364	1	203.3559	0
2.020564	2	205.4485	1
2.106765	0	207.5411	1
2.192965	1	209.6336	0
2.279166	1	211.7262	0
2.365367	0	213.8188	0
2.451567	1	215.9114	1
2.537768	0	218.0039	1
2.623968	0	220.0965	0
2.710169	0	222.1891	0
2.796369	1	224.2817	0
2.88257	0	226.3742	0
2.968771	0	228.4668	0
3.054971	0	230.5594	0
3.141172	0	232.6519	2
3.227372	0	234.7445	1
3.313573	8	236.8371	0
3.399774	24	238.9297	0
3.485974	84	241.0222	0
3.572175	111	243.1148	0
3.658375	105	245.2074	0
3.744576	186	247.3	0
3.830776	325	249.3925	0
3.916977	512	251.4851	0
4.003178	437	253.5777	0
4.089378	207	255.6703	0
4.175579	38	257.7628	0
More	7	More	1

Appendix Table 14: Histogram of location 7 air flow directional degrees and velocity (m/s)

Location 8:



Appendix Figure 15: Graphical data of velocity direction in degrees over time for the three test repeats



Appendix Figure 16: Graphical data of air velocity magnitude (m/s) over time for the three test repeats

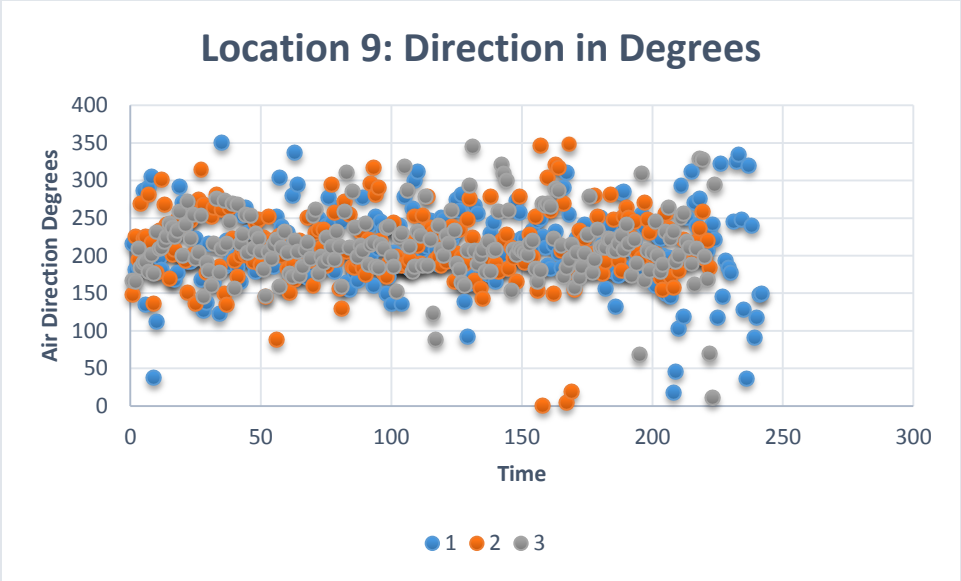
<i>Location 8 Velocity</i>		<i>Location 8 Degree</i>	
Mean	0.592371	Mean	216.0503
Standard Error	0.015644	Standard Error	4.071941
Median	0.513128	Median	220.0172
Mode	0.170294	Mode	330.0001
Standard Deviation	0.408853	Standard Deviation	106.4172
Sample Variance	0.167161	Sample Variance	11324.62
Kurtosis	1.856655	Kurtosis	-0.85355
Skewness	1.219458	Skewness	-0.50633
Range	2.394098	Range	359.3015
Minimum	0.018204	Minimum	0.629969
Maximum	2.412302	Maximum	359.9315
Sum	404.5893	Sum	147562.4
Count	683	Count	683
Confidence Level(95.0%)	0.030717	Confidence Level(95.0%)	7.995046

Appendix Table 15: Statistical breakdown of location 8 air flow directional degrees and velocity (m/s)

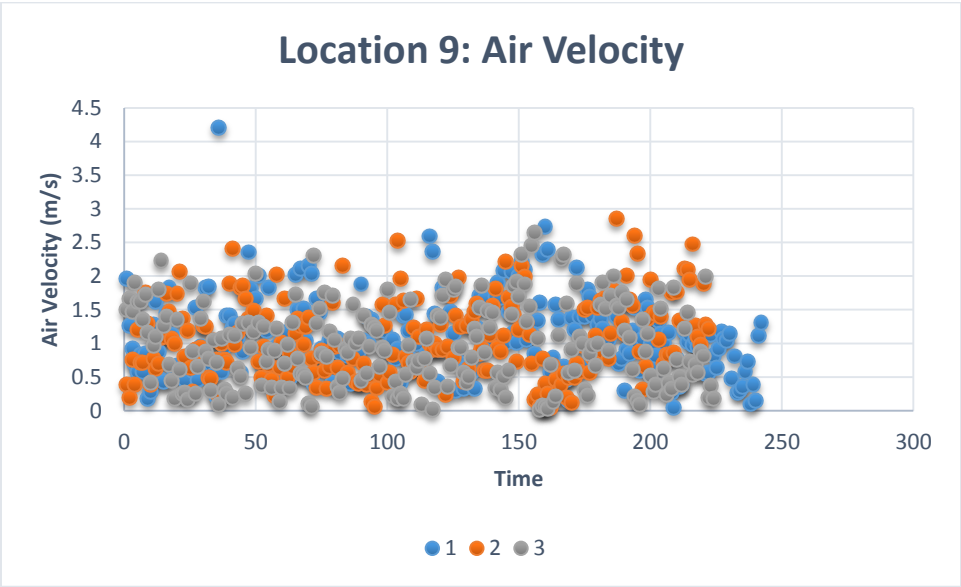
Location 8: Velocity		Location 8: Degree	
<i>Bin</i>	<i>Frequency</i>	<i>Bin</i>	<i>Frequency</i>
0.018204	1	0.629969	1
0.110284	44	14.44926	28
0.202365	64	28.26855	23
0.294446	63	42.08784	23
0.386527	74	55.90713	15
0.478607	73	69.72642	15
0.570688	63	83.5457	8
0.662769	60	97.36499	6
0.754849	45	111.1843	14
0.84693	48	125.0036	11
0.939011	38	138.8229	11
1.031092	27	152.6422	11
1.123172	10	166.4614	20
1.215253	14	180.2807	32
1.307334	16	194.1	43
1.399414	6	207.9193	50
1.491495	11	221.7386	32
1.583576	7	235.5579	21
1.675657	5	249.3772	22
1.767737	2	263.1965	26
1.859818	3	277.0158	17
1.951899	3	290.835	32
2.043979	1	304.6543	23
2.13606	1	318.4736	36
2.228141	1	332.2929	64
2.320222	2	346.1122	46
More	1	More	53

Appendix Table 16: Histogram of location 8 air flow directional degrees and velocity (m/s)

Location 9:



Appendix Figure 17: Graphical data of velocity direction in degrees over time for the three test repeats



Appendix Figure 18: Graphical data of air velocity magnitude (m/s) over time for the three test repeats

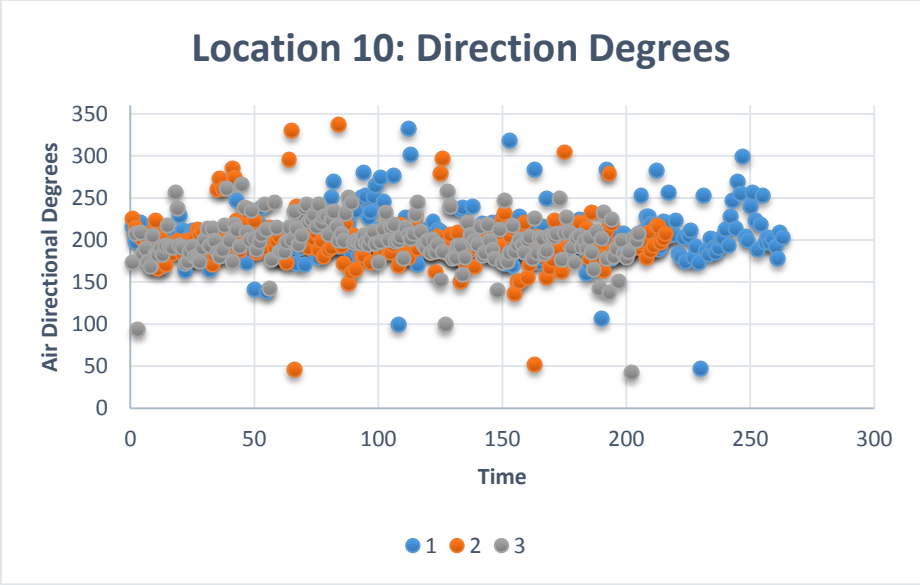
<i>Location 9 Air Velocity</i>		<i>Location 9 Directional Degree</i>	
Mean	1.037884	Mean	211.5215
Standard Error	0.022055	Standard Error	1.839078
Median	0.97811	Median	207.5005
Mode	0.572713	Mode	178.5347
Standard Deviation	0.578505	Standard Deviation	48.23857
Sample Variance	0.334668	Sample Variance	2326.96
Kurtosis	0.788893	Kurtosis	2.471597
Skewness	0.655464	Skewness	-0.38433
Range	4.199915	Range	349.261
Minimum	0.011795	Minimum	0.963992
Maximum	4.21171	Maximum	350.225
Sum	714.0642	Sum	145526.8
Count	688	Count	688
Confidence Level(95.0%)	0.043304	Confidence Level(95.0%)	3.610889

Appendix Table 17: Statistical breakdown of location 9 air flow directional degrees and velocity

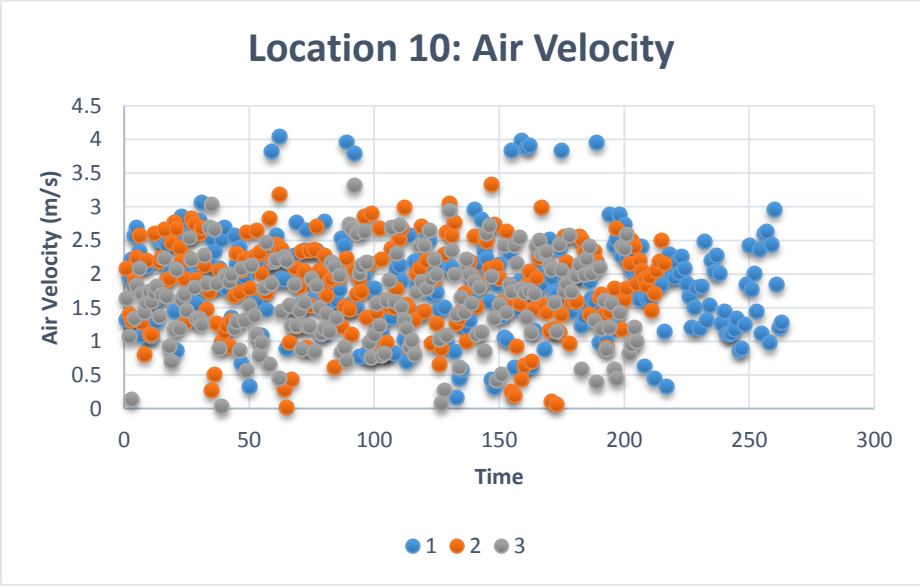
Location 9 Velocity		Locaiton 9 Degree	
<i>Bin</i>	<i>Frequency</i>	<i>Bin</i>	<i>Frequency</i>
0.011795	1	0.963992	1
0.17333	23	14.39711	2
0.334865	46	27.83022	2
0.496401	60	41.26333	2
0.657936	75	54.69645	1
0.819471	65	68.12956	0
0.981006	75	81.56268	2
1.142541	74	94.99579	4
1.304076	62	108.4289	1
1.465612	51	121.862	4
1.627147	39	135.2951	6
1.788682	38	148.7282	16
1.950217	33	162.1614	28
2.111752	20	175.5945	36
2.273287	8	189.0276	93
2.434823	9	202.4607	106
2.596358	3	215.8938	96
2.757893	4	229.3269	77
2.919428	1	242.76	54
3.080963	0	256.1932	49
3.242498	0	269.6263	33
3.404034	0	283.0594	29
3.565569	0	296.4925	16
3.727104	0	309.9256	9
3.888639	0	323.3587	12
4.050174	0	336.7918	4
More	1	More	5

Appendix Table 18: Histogram of location 9 air flow directional degrees and velocity (m/s)

Location 10:



Appendix Figure 19: Graphical data of velocity direction in degrees over time for the three test repeats



Appendix Figure 20: Graphical data of air velocity magnitude (m/s) over time for the three test repeats

<i>Location 10 Velocity</i>		<i>Location 10 Degree</i>	
Mean	1.777256	Mean	201.4132
Standard Error	0.026172	Standard Error	1.146698
Median	1.809495	Median	199.2518
Mode	1.597028	Mode	220.9981
Standard Deviation	0.684496	Standard Deviation	29.99004
Sample Variance	0.468534	Sample Variance	899.4025
Kurtosis	0.385845	Kurtosis	6.516893
Skewness	0.097763	Skewness	0.047269
Range	4.020791	Range	295.0763
Minimum	0.02	Minimum	42.39526
Maximum	4.040792	Maximum	337.4716
Sum	1215.643	Sum	137766.6
Count	684	Count	684
Confidence Level(95.0%)	0.051388	Confidence Level(95.0%)	2.251476

Appendix Table 19: Statistical breakdown of location 10 air flow directional degrees and velocity

Location 10 Velocity		Location 10 Degree	
<i>Bin</i>	<i>Frequency</i>	<i>Bin</i>	<i>Frequency</i>
0.02	1	42.39526	1
0.174646	6	53.74435	3
0.329292	8	65.09344	0
0.483938	9	76.44253	0
0.638584	12	87.79162	0
0.79323	11	99.14071	1
0.947875	35	110.4898	3
1.102521	30	121.8389	0
1.257167	46	133.188	0
1.411813	41	144.5371	7
1.566459	58	155.8862	7
1.721104	48	167.2352	13
1.87575	60	178.5843	50
2.030396	67	189.9334	121
2.185042	63	201.2825	169
2.339688	55	212.6316	141
2.494333	36	223.9807	76
2.648979	42	235.3298	28
2.803625	27	246.6789	19
2.958271	10	258.028	17
3.112917	6	269.3771	7
3.267563	1	280.7261	8
3.422208	2	292.0752	4
3.576854	0	303.4243	4
3.7315	0	314.7734	1
3.886146	5	326.1225	1
More	5	More	3

Appendix Table 20: Histogram of location 10 air flow directional degrees and velocity (m/s)